Journal of Catalysis 268 (2009) 181–195

Contents lists available at ScienceDirect

Journal of Catalysis

journal homepage: www.elsevier.com/locate/jcat

Hydrogenation of acetylene–ethylene mixtures over Pd and Pd–Ag alloys: First-principles-based kinetic Monte Carlo simulations

Donghai Mei [a,b], Matthew Neurock [b,*], C. Michael Smith [c]

[a] Institute for Interfacial Catalysis, Pacific Northwest National Laboratory, Richland, WA 99352, USA
[b] Department of Chemical Engineering and Chemistry, University of Virginia, Charlottesville, VA 22904, USA
[c] The Dow Chemical Company, Freeport, TX 77541, USA

ARTICLE INFO

Article history:
Received 7 May 2009
Revised 29 August 2009
Accepted 6 September 2009
Available online 22 October 2009

Keywords:
Selective hydrogenation
Kinetics
Density functional theory
Kinetic Monte Carlo
Pd/Ag alloys
Acetylene–ethylene mixtures

ABSTRACT

The kinetics for the selective hydrogenation of acetylene–ethylene mixtures over model Pd(1 1 1) and bimetallic Pd–Ag alloy surfaces were examined using first principles-based kinetic Monte Carlo (KMC) simulations to elucidate the effects of alloying and reaction conditions. The elementary steps that control the selective and unselective pathways, including hydrogenation, dehydrogenation, and C–C bond breaking, were analyzed using first-principle density functional theory (DFT) calculations. The results were used to construct an intrinsic kinetic database that was used in a variable time step kinetic Monte Carlo simulation to follow the kinetics and the molecular transformations in the selective hydrogenation of acetylene–ethylene feeds over Pd and Pd–Ag surfaces. Through-surface and through-space lateral interactions between coadsorbates were estimated using DFT-parameterized bond order conservation and van der Waal interaction models, respectively. The simulations show that the rate of acetylene hydrogenation as well as ethylene selectivity increases with temperature over both the Pd(1 1 1) and the Pd–Ag/Pd(1 1 1) alloy surfaces. The selective hydrogenation of acetylene to ethylene proceeds via the formation of a surface vinyl intermediate. The unselective formation of ethane is the result of the over-hydrogenation of ethylene as well as over-hydrogenation of vinyl to form ethylidene. Ethylidene further hydrogenates to form ethane and dehydrogenates to form ethylidyne. While ethylidyne is not reactive, it can block adsorption sites and thus limit the availability of hydrogen on the surface which enhances the selectivity. Alloying Ag into the Pd surface decreases the overall rate but increases the ethylene selectivity significantly by promoting the selective hydrogenation of vinyl to ethylene and concomitantly suppressing the unselective path involving the hydrogenation of vinyl to ethylidene and the dehydrogenation of ethylidene to ethylidyne. This is consistent with experimental results which suggest that only the predominant hydrogenation path which involves the sequential addition of hydrogen to form vinyl and ethylene exists over the Pd–Ag alloys. Ag enhances the desorption of ethylene and hydrogen from the surface thus limiting their ability to undergo subsequent reactions. The simulated apparent activation barriers were calculated to be 32–44 kJ/mol on Pd(1 1 1) and 26–31 kJ/mol on Pd–Ag/Pd(1 1 1), respectively. The reaction was found to be essentially first order in hydrogen and −0.4 and −0.21 order in acetylene over Pd(1 1 1) and Pd–Ag/Pd(1 1 1) surfaces, respectively. The results reveal that increases in the hydrogen partial pressure increase the activity but decrease ethylene selectivity over both Pd and Pd–Ag/Pd(1 1 1) surfaces.

1. Introduction

Polymer-grade ethylene is currently produced via the selective hydrogenation of acetylene present at 0.5–2% by volume from crude ethylene streams that exit the naphtha steam cracker down to levels below 5 ppm. This is typically carried out in a fixed-bed reactor over supported Pd and Pd–Ag catalysts. Current ethylene plants operate in either front- or tail-end configurations. In the front-end process, the ethylene hydrogenation unit is placed before the de-methanizer unit. The feedstocks typically contain higher hydrogen and lighter hydrocarbon compositions and result in very high rates of hydrogenation. The temperatures must be closely maintained within a very narrow operating window of 323–363 K in order to minimize the over-hydrogenation that can lead to significant loss of selectivity and potential reaction runaway. In the tail-end process, the hydrogenation unit is located further downstream just after the de-ethanizer and operates at significantly lower partial pressures of hydrogen. The lower hydrogen levels tend to result in carbon deposits, green oil formation, and

* Corresponding author. Fax: +1 434 982 2658.
E-mail address: mn4n@virginia.edu (M. Neurock).

0021-9517/$ - see front matter © 2009 Elsevier Inc. All rights reserved.
doi:10.1016/j.jcat.2009.09.004

faster rates of catalyst deactivation. Thus the predominant issue that plagues both the front-end and tail-end processes is the hydrogenation selectivity to ethylene [1–4].

The selectivity to ethylene is thought to be controlled by either thermodynamic considerations where by the more strongly bound acetylene displaces ethylene from the surface or by kinetic considerations where ethylene desorbs before it can hydrogenate. A detailed understanding of the fundamental kinetics will help to elucidate which of these factors dominate and under what conditions. The intrinsic kinetics for this system, however, have been difficult to discern since the catalytic activity and selectivity are influenced by the range of variables including the gas phase composition [5–10], catalyst particle size and dispersion [2,6,11–14], presence of carbonaceous surface intermediates [15–20], hydride and carbide formation [1,21–23], catalyst support [7,24], and the addition of promoters such as CO [2,25–28]. These features influence the surface coverage of acetylene and other hydrocarbon intermediates as well as the availability of hydrogen which can significantly influence both the activity and selectivity. The experimentally reported apparent activation energies for the hydrogenation of acetylene over Pd have been reported to be between 40 and 70 kJ/mol [5,11,13]. The acetylene and hydrogen reaction orders were reported to be within the range between 0 to –0.5 and 0.5 to 1.5, respectively [3,4].

Although Pd is active, its selectivity to ethylene at high acetylene conversions is rather low. The selectivity can be significantly improved by alloying Pd with Ag [29–38]. Jin et al. demonstrated significant improvement in the catalytic selectivity over Pd–Ag alloys but required that the catalysts be activated by a high temperature reduction in hydrogen [32]. They suggested that this reduction results in uniformly dispersed Ag within the surface layer that breaks apart larger Pd ensembles. They demonstrated this by monitoring the CO stretching frequencies which showed the migration of CO from the bridge to the atop sites upon high temperature reduction of the Pd–Ag alloy in hydrogen. More detailed STM studies by Khan et al. over model Pd–Ag particles confirmed that Pd and Ag are uniformly dispersed in the active surface [37]. The promotional effects of Ag have been attributed to classical electronic and ensemble effects that occur upon alloying an active metal with a group IB metal. The addition of Ag into Pd increases the electron density of the Pd d-band as a result of charge transfer from Ag to Pd [35]. We have shown previously that these electronic effects weaken the adsorption of both ethylene and acetylene on the alloy surface [39]. The electronic and ensemble effects decrease the acetylene binding energy by 10–20 kJ/mol, and 30–40 kJ/mol, respectively. This should favor both thermodynamic and kinetic considerations as the weaker metal–adsorbate bond strength promotes both desorption and hydrogenation. Recent theoretical calculations are consistent with this picture [31,35]. Despite the progress in understanding these elementary steps, little can be concluded concerning the influence of Ag on the actual selectivity without a more rigorous following of the rates of the elementary steps since Ag will influence both desorption and hydrogenation of acetylene and ethylene which ultimately controls the selectivity.

The intrinsic effects of alloying Pd with Ag have been difficult to interpret as they are typically followed by monitoring changes in macroscopic kinetics and overall reaction selectivity. The selectivity, for example, shows marked improvements when Ag is added to Pd but the actual composition of Ag was found to have a rather weak influence on the selectivity. Bond et al., for example, showed that ethylene selectivity decreased by less than 1% as the Ag bulk composition increased from 10% to 30% [40]. The changes in the elementary step kinetics, however, are thought to be more sensitive to the composition of Ag in the alloy as there are differences in the activity and other kinetic variables such as the reaction orders. Hydrogen reaction orders, for example, were found to increase from 1.68 for 10% and 20% Pd–Ag alloys to 1.80 for 30% Pd–Ag alloys. The effect of temperature on the addition of Ag and the increasing composition of Ag in the alloy were found to have a significant influence on the selectivity. The increase in temperature was found to decrease the selectivity more rapidly than the increase in hydrogen partial pressure. Recent temperature-programed desorption (TPD) experiments showed a decrease in the overall catalytic activity and an increase in the selectivity on model Pd–Ag particles supported on an alumina. Ag was thought to control the amount of subsurface hydrogen and thus prevent the over-hydrogenation pathways to ethane [37].

Despite the rigorous efforts which have provided a wealth of information on some of the elementary processes [41–44], our understanding of the mechanism and the intrinsic kinetics that govern the selective hydrogenation of acetylene–ethylene mixtures over the Pd–Ag alloys is still rather incomplete [1,2]. While various reaction mechanisms and kinetic models have been proposed to fit the experimental results for pure Pd, these models are typically regressed from experiment and as such are only applicable to within the range of operating conditions that the experiments were carried out. In addition, they also tend to be dependent upon the specific catalyst and catalyst preparation that is used [1–4]. In order to develop models with potentially predictive capabilities, a more detailed understanding of the molecular transformations that occur at the catalyst surface, and the influence of the atomic surface structure of the catalyst will be required to elucidate the catalytic features that ultimately control the catalytic activity and selectivity for the selective hydrogenation of acetylene.

Kinetic Monte Carlo (KMC) simulations have been successfully used to overcome a number of the limitations of conventional deterministic models as they can explicitly include the atomic surface structure and thus track molecular transformations as a function of time and reaction conditions. We have previously developed and applied first-principles-based kinetic Monte Carlo simulations to examine the hydrogenation of pure ethylene and pure acetylene over the pure Pd(1 1 1) surface [45–48]. In the present work, we adopt this first-principles-based KMC approach to simulate the kinetics for the selective hydrogenation of tail-end acetylene/ethylene mixtures over the Pd(1 1 1) and the bimetallic Pd–Ag/Pd(1 1 1) surfaces in order to elucidate the influence of alloying on the elementary kinetics and the macroscopic kinetic behavior.

2. Simulation details

2.1. Reaction mechanism

The selective hydrogenation of acetylene to ethylene is thought to proceed via a Horiuti–Polanyi mechanism involving the successive addition of hydrogen to convert acetylene to vinyl and vinyl to ethylene [49]. The reaction proceeds via the dissociative adsorption of hydrogen and the chemisorption of acetylene at higher fold coordination sites. This is thought to be the primary path to ethylene and the major unselective path to ethane. A secondary path to ethane exists via the hydrogenation of the vinyl intermediate to ethylidene which can subsequently hydrogenate to form ethane.

A number of other secondary C_2 surface intermediates such as ethylidyne and vinylidene are known to form on Pd(1 1 1) [41,50–57] and are also likely present under reaction conditions. These secondary surface intermediates act either as spectator species to block the active sites or as precursors to oligomerization which results in the formation of green oils and benzene under high pressures [16,18,58]. At higher temperatures, the adsorbed acetylene and ethylene can decompose into CH and CH_2 intermediates

(C_1) as a result of the activation of the C–C bond [51]. The adsorption and reaction for all these intermediates were also considered in this work.

In previously reported work, we examined the hydrogenation of pure acetylenic feeds over Pd(1 1 1) and only considered the primary hydrogenation paths. The dehydrogenation and decomposition paths were assumed to have little effect on the overall activity and selectivity over pure Pd at the lower temperatures of interest and were therefore not considered. These paths, however, are important in the formation of ethane and may also play a role in controlling the surface coverages which influence hydrogen availability. Herein, we extend our previous simulations of pure acetylene feeds over Pd(1 1 1) to the simulations of the tail-end acetylene/ethylene mixtures. We explicitly include all the secondary surface intermediates (C_1 and C_2) species, the corresponding unselective dehydrogenation reaction steps for acetylene to acetylidene, vinyl to vinylidene, ethylidyne to vinylidene, ethyl to ethylidyne, as well as four C–C bond-breaking paths. The proposed mechanism examined is given in Fig. 1. While we provide for a detailed accounting of the surface chemistry, we have not explicitly included in the present simulations oligomerization reactions that can lead to green oil or the influence of subsurface hydrogen [1,2] and carbon [1,21–23] which are known to be present. Such simulations will require a considerable number of theoretical calculations which is beyond the focus of the work presented herein.

2.2. Intrinsic kinetics calculations

The intrinsic kinetics which govern the elementary steps involved in the selective and unselective pathways for acetylene and ethylene hydrogenation over Pd(1 1 1) and Pd–Ag/Pd(1 1 1) alloy surfaces were calculated previously using gradient-corrected plane wave density functional theory (DFT) calculations implemented in the Vienna ab initio Simulation Program (VASP) [59,60]. The results are compiled here to construct an extensive intrinsic kinetic database covering the proposed reaction paths involved for the selective hydrogenation of acetylene–ethylene mixtures. A more in-depth discussion was given in previous publications [39,57]. The errors that arise from DFT calculations are typically less than 20 kJ/mol [61–63]. Many of the deviations and errors cancel out in taking energy differences which tend to improve calculated activation barriers. There are still likely some deviations though in the accuracy in the calculated rate constants for individual steps. As such we focus herein instead on the changes that result from the kinetics rather than quantitative predications. The barriers for all the primary pathways were calculated directly using DFT. The barriers for a few of the secondary C–C activation steps were determined using DFT-parameterized bond order conservation (BOC) method [45,46,48,64–67]. The intrinsic kinetic database includes (1) the binding energies and atomization energies (Table 1), as well as the geometric structures of all surface intermediates; (2) reaction energies and activation barriers (Table 2) for the elementary steps considered in the reaction mechanism presented in Fig. 1. The values estimated from DFT-parameterized BOC method are also given in Table 2. The intrinsic elementary step kinetics are thus determined directly within the simulations from this intrinsic database.

The model Pd and PdAg (1 1 1) surfaces used herein are rather simplified in that they do not examine the effects of structure, support or the presence or formation of subsurface hydrides and carbons. While subsurface carbon [6–9] and hydrogen [1,2] influence the selectivity of supported Pd, their effects on PdAg alloys have yet to be established. Recent results by Khan et al. [37], for example, show that the addition of Ag into Pd shuts down the formation of subsurface hydrogen and prevents the formation of the hydride phase. Similar alloying effects may also prevent subsurface carbide formation. Regardless, we do not analyze these effects and instead focus solely on the influence of alloying on the surface hydrogenation kinetics. Despite its simplicity the model provides for the essential heterogeneity to understand the initial influence of alloying.

In this work we examine the pure Pd(1 1 1) surface as well as the two specific $Pd_{50\%}Ag_{50\%}$ alloys on the Pd(1 1 1) substrate presented in Fig. 2 which were chosen to mimic those proposed by Jin et al. [10] At high reduction temperature, the Pd and Ag are thought to be uniformly distributed such as that shown in Fig. 2b. The second $Pd_{50\%}Ag_{50\%}$ structure shown in Fig. 2c examined the formation of small Pd and Ag ensembles (Pd_3 and Ag_3) which can form at lower reduction temperature. The well-dispersed alloy shown in Fig. 2b is thermodynamically more stable than ensemble structure shown in Fig. 2c. This is consistent with the recent STM results [37].

The DFT-calculated binding energies for all the adsorbates on the Pd(1 1 1) as well as on the Pd–Ag alloy surfaces considered in

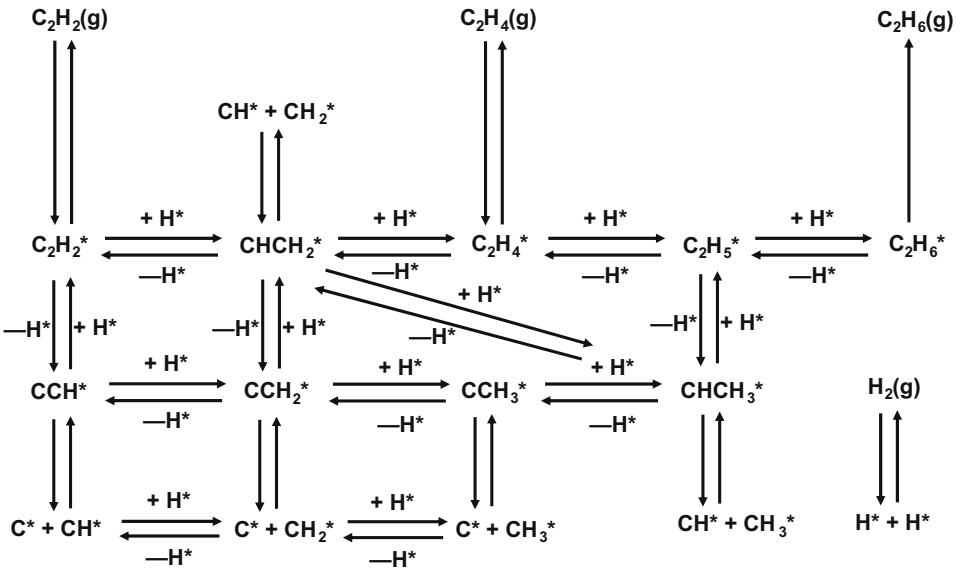

Fig. 1. Selective and unselective reaction pathways for the hydrogenation of acetylene.

Table 1
DFT-calculated atomization energies and binding energies for all the surface intermediates considered in the selective hydrogenation of acetylene–ethylene mixtures over the Pd(1 1 1) and the bimetallic Pd–Ag/Pd(1 1 1) surfaces.

Species	Atomization[a] energy (kJ/mol)	Binding energy (kJ/mol)					
		Pd(1 1 1)			Pd–Ag/Pd(1 1 1)		
		Atop	Bridge	Hollow	Atop	Bridge	Hollow
H	0	−187	−232	−260	–	−258	–
H_2	436	–	–	–	–	–	–
C	0	–	–	−638	–	–	−546
CH	324	–	–	−631	–	–	−555
CH_2	824	–	−365	–	–	−344	–
CH_3	1306	−172	–	–	−162	–	–
CCH	1167	–	–	−405	–	−329	–
CCH_2	1374	–	–	−537	–	–	−439
CCH_3	1590	–	–	−638	–	–	−557
C_2H_2	1746	–	−136	−172	–	−126	–
$CHCH_2$	1907	–	–	−274	−214	–	–
$CHCH_3$	2102	–	−330	–	–	−315	–
C_2H_4	2398	−27	−82			−70	
C_2H_5	2566	−154	–	–	−135	–	–
C_2H_6	3005	−5	−5	–	−5	−5	–

[a] ZPE corrections to the atomization energies were calculated using DFT. It is well recognized that DFT tends to overestimate these values. The DFT-BOC estimation method used, however, calculates only the overall energy difference between reactants and products. As such, the overestimation tends to cancel out. We ran a sequence of test simulations with ZPE values taken directly from the NIST database and found errors of less than 2% in the simulated activation energies and surface coverages.

Table 2
DFT-calculated and DFT-BOC estimated reaction energies ΔH and activation barriers ΔE^* of the elementary reactions over the Pd(1 1 1) and the bimetallic Pd–Ag/Pd(1 1 1) surfaces.

No.	Elementary reaction	Pd(1 1 1)		Pd–Ag/Pd(1 1 1)	
		ΔE^* (kJ/mol)	ΔH (kJ/mol)[a]	ΔE^* (kJ/mol)	ΔH (kJ/mol)[a]
1	$H_2(g) + 2^* \leftrightarrow H^* + H^*$	[b]	82[d]	[b]	77[d]
2	$C_2H_2(g) + * \leftrightarrow C_2H_2^*$	[b]	172[c]	[b]	126[c]
3	$C_2H_4(g) + * \leftrightarrow C_2H_4^*$	[b]	82[c]	[b]	70[c]
4	$C_2H_2^* + H^* \leftrightarrow CHCH_2^* + *$	66[c]	26[c]	66[c]	+7[c]
5	$CHCH_2^* + H^* \leftrightarrow C_2C_4^* + *$	74[c]	58[c]	10[c]	92[c]
6	$C_2H_4^* + H^* \leftrightarrow C_2C_5^* + *$	72[c]	+20[c]	61[c]	+20[c]
7	$C_2H_5^* + H^* \rightarrow C_2H_6(g) + 2^*$	71[c]	30[c]	78[c]	33[c]
8	$C_2H_2^* + * \leftrightarrow CCH^* + H^*$	181[c]	73[c]	212[c]	+121[c]
9	$CHCH_2^* + * \leftrightarrow CCH_2^* + H^*$	127[c]	+20[c]	147[c]	+52[c]
10	$CHCH_2^* + H^* \leftrightarrow CHCH_3^* + *$	85[c]	+60[c]	73[c]	5[c]
11	$CHCH_2^* + * \leftrightarrow CH_2^* + CH^*$	220[c]	+111[c]	181[c]	+139[c]
12	$CCH_2^* + H^* \leftrightarrow CCH_3^* + *$	39[d]	56[c]	44[d]	76[c]
13	$CCH_3^* + H^* \leftrightarrow CHCH_3^* + *$	120[d]	+53[c]	102[d]	+43[c]
14	$CCH^* + H^* \leftrightarrow CCH_2^* + *$	93[d]	72[c]	42[d]	60[c]
15	$CCH^* + {}^* \leftrightarrow C^* + CH^*$	148[d]	7[c]	173[d]	+85[c]
16	$CCH_2^* + * \leftrightarrow C^* + CH_2^*$	158[d]	+84[d]	155[d]	+99[d]
17	$CCH_3^* + * \leftrightarrow C^* + CH_3^*$	124[d]	+112[d]	133[d]	0[d]
18	$CHCH_3^* + * \leftrightarrow CH^* + CH_3^*$	67[d]	2[d]	98[d]	+55[c]
19	$CH^* + {}^* \leftrightarrow C^* + H^*$	121[d]	+50[c]	125[d]	+68[c]
20	$CH^* + H^* \leftrightarrow CH_2^* + *$	105[d]	+17[c]	72[d]	39[c]
21	$CH_2^* + H^* \leftrightarrow CH_3^* + *$	62[d]	28[c]	53[d]	41[c]
22	$C_2C_5^* + * \leftrightarrow CHCH_3^* + H^*$	87[d]	+4[c]	84[d]	+26[c]

Note: [a]The reverse barriers for the elementary reaction steps are calculated by $\Delta E^* - \Delta H$.
[b] The barriers for adsorption of acetylene and ethylene, as well as for dissociative adsorption of hydrogen over the Pd(1 1 1) and the bimetallic Pd–Ag/Pd(1 1 1) surfaces are assumed to be negligible.
[c] DFT calculations [39,56,57].
[d] DFT-BOC estimation.

the simulations are given in Table 1. The results in Table 1 show that the addition of Ag into the Pd surface weakens the metal–adsorbate bond strength for all the hydrocarbon intermediates as a result of electronic (ligand) as well as geometric (ensemble) effects. Ensemble effects lead to a greater weakening of the metal–adsorbate bond as a result of change in adsorbate site preference. The adsorption of acetylene, for example, shifts from the 3-fold fcc site on the Pd(1 1 1) surface to the Pd–Pd bridge site on the $Pd_{50\%}Ag_{50\%}$/Pd(1 1 1) alloy surface at 0.25 ML coverage, resulting in a decrease in the chemisorption energy from −172 kJ/mol on the Pd(1 1 1) surface to −126 kJ/mol on the $Pd_{50\%}Ag_{50\%}$/Pd(1 1 1) surface. Similarly, the most favorable binding site for the vinyl intermediate changes from the η_1–η_2 binding configuration at the 3-fold fcc site on Pd(1 1 1) to the atop site Pd site on the Pd–Ag/Pd(1 1 1) alloy surface. The binding energy of the vinyl species is weakened from −274 kJ/mol on the Pd(1 1 1) surface to −214 kJ/mol on the Pd–Ag/Pd(1 1 1) surface.

The elementary reaction energies were calculated as the total electronic energy difference between the product state and the reactant state ($\Delta E_{rxn} = \Delta E_{products} - \Delta E_{reactants}$). A negative value for the reaction energy refers to an exothermic reaction. The DFT-calculated reaction energies and activation barriers for the

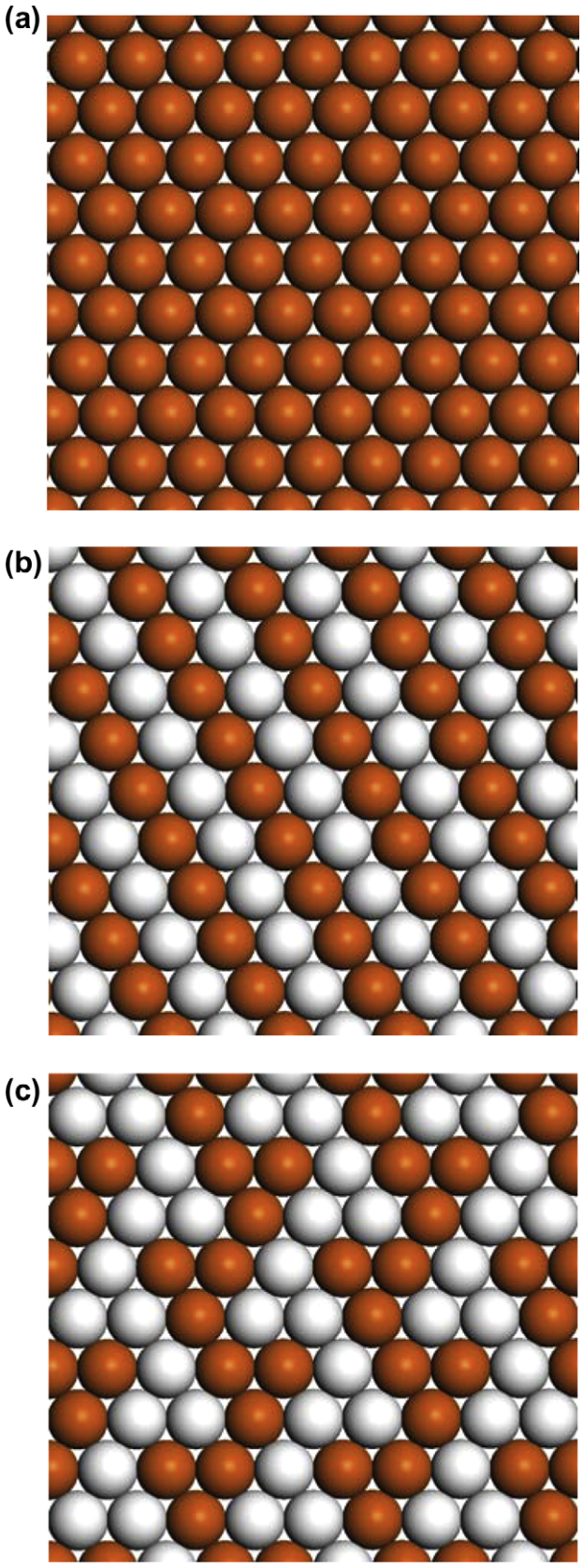

Fig. 2. The catalytic surfaces used in the kinetic Monte Carlo simulations. (a) Pd(1 1 1); (b) uniformly dispersed $Pd_{50\%}Ag_{50\%}$/Pd(1 1 1); and (c) triangular ensemble $Pd_{50\%}Ag_{50\%}$/Pd(1 1 1). The orange spheres and the white spheres represent Pd and Ag atoms, respectively. (For interpretation of the references to colour in this figure legend, the reader is referred to the web version of this article.)

elementary reaction steps considered herein for the selective hydrogenation of acetylene over both the Pd(1 1 1) and the Pd–Ag/Pd(1 1 1) alloy surface are reported in Table 2. The reaction energies for most of the hydrogenation steps were found to be exothermic, whereas those for dehydrogenation were found to be endothermic. This suggests that the bond-making (hydrogenation) reactions were more favorable than the bond-breaking (dehydrogenation) steps. This trend was more pronounced for the reactions carried out over the Pd–Ag alloy surfaces. The reaction energy for ethylene hydrogenation to ethyl, for example, was found to be endothermic by +20 kJ/mol on Pd(1 1 1). This reaction over the $Pd_{50\%}Ag_{50\%}$/Pd(1 1 1) alloy surface, however, was exothermic by 20 kJ/mol. The intrinsic activation barriers were calculated using the nudged elastic band approach [68] implemented in VASP [59,60] for the elementary reaction steps over both the Pd(1 1 1) and $Pd_{50\%}Ag_{50\%}$/Pd(1 1 1) alloy surfaces [39,57]. The intrinsic activation barriers for the four steps in the hydrogenation of acetylene to ethane on the Pd(1 1 1) surface

$$CH{\equiv}CH^{*} + 4H^{*} \xrightarrow{1} CH_2{=}CH^{*} + 3H^{*} \xrightarrow{2} CH_2{=}CH_2^{*} + 2H^{*} \xrightarrow{3} CH_3{-}CH_2^{*} + H^{*} \xrightarrow{4} CH_3{-}CH_3$$

were calculated to be 66, 74, 72, and 71 kJ/mol, respectively. The intrinsic barrier for vinyl hydrogenation to ethylidene over the Pd(1 1 1) surface was calculated to be 85 kJ/mol. It was found that alloying Pd with Ag weakly decreased all these barriers with the exception of the hydrogenation of vinyl to ethylene where the barrier decreased by 64 kJ/mol as a result of the change in the adsorption site for vinyl upon alloying Pd with Ag. The details of the calculations and the geometrical information were described in previous publications [39,56,57]. The results are also in agreement with other recent theoretical results [31,35].

Surface coverages and the local environment around the active reaction sites were found to have a significant impact on the intrinsic hydrogenation kinetics. DFT results predict that the activation barrier for acetylene hydrogenation to vinyl decreases from 66 kJ/mol at 0.25 ML coverage to 50 kJ/mol at 0.33 ML surface coverage. The overall reaction energy drops from −26 kJ/mol to −43 kJ/mol as the coverage is increased [57]. Surface coverage on the intrinsic kinetics was accounted for within the KMC simulation via *through-space* and *through-surface* lateral interaction models. The *through-space* interactions between specific pairs of neighboring adsorbates which are a direct function of their intra- and intermolecular distances as well as their intermolecular orientations were calculated using the van der Waals model (vdW) used in the Merck Molecular Force Field (MMFF94) [69]. The *through-surface* interactions, arising from metal–atom sharing or adsorbate-bond sharing, were determined from a bond order conservation (BOC) model that was fit to matching DFT calculations on the adsorption and reaction energies carried out at different coverages [45,46,48,64–67]. The DFT-calculated activation barriers and reaction energies presented in Table 2 were used directly in the simulations but augmented by the BOC and the vdW models to account for the coverage effects.

2.3. Kinetic Monte Carlo approach

The intrinsic kinetics derived from DFT calculations together with the DFT-scaled lateral interaction models accounted for the *through-space* and *through-surface* interaction were used as the input to kinetic Monte Carlo simulation to allow us to track the spatial–temporal molecular transformations over the metal surface as a function of reaction time and process conditions. The details of this DFT-based KMC approach have been reported in previous pub-

lications [45,46,48,64–67]. A brief summary of this approach is given below.

The simulations follow the site-explicit pathways for adsorption, desorption, surface diffusion, and surface reaction over well-defined (1 1 1) surfaces which are represented by a periodic 32×32 metal atom grid containing 6144 surface sites with periodic boundary conditions. The DFT-calculated intrinsic kinetic database, the DFT-scaled BOC and MMFF models, along with the reaction condition (temperature and partial pressures) provide the necessary input for the simulations. All the surface sites are examined at each time step within the simulation in order to construct a cumulative rate probability distribution for all the possible surface processes (adsorption, surface reaction, surface diffusion, and desorption) that can occur within the chosen time step. Diffusion can either be explicitly simulated, neglected or treated as quasi-equilibrated. We have chosen to treat the diffusion of surface intermediates herein as being quasi-equilibrated. We had previously examined the influence of diffusion on the hydrogenation of ethylene and found that it did not significantly influence the results [46,47]. The reaction rates for elementary steps such as surface reaction, desorption, and diffusion are calculated using transition state theory, where the rate is given by:

$$r_i = v_i \exp\left(\frac{-\Delta E_i}{RT}\right) \tag{1}$$

in which v_i is the pre-exponential factor, R is the gas constant, T is the reaction temperature, and ΔE_i is the activation energy barrier for the elementary reaction i. The pre-exponential factors, v_i, were determined from statistical mechanical estimates [70,71]. A theoretical value of 10^{13} s^{-1} was chosen for all unimolecular and immobile surface reactions and desorption steps. For adsorption, the sticking coefficients were used instead of the pre-exponential factors. The adsorption rate for species i was determined from the following expression:

$$r_{\mathrm{ad},i} = s_0 \cdot P_i \cdot A_S \cdot (2\pi \cdot MW_i \cdot RT)^{-0.5} \cdot \exp\left(\frac{-\Delta E_i}{RT}\right) \tag{2}$$

in which s_0, P_i, MW_i, and A_s are the sticking coefficient, the partial pressure of species i, the molecular weight of i, and the surface area of the site(s) involved. The sticking coefficients of acetylene, ethylene, and hydrogen were taken to be 1.0, 1.0, and 0.1, respectively. These values are based on previous experimental results and a microkinetic modeling analysis [72,73].

The variable time step kinetic Monte Carlo algorithm proceeds in event space whereby the time is updated after each event. As such there is only one event per time step but the time step for each event can vary. The rates for all processes at a given instant in time are added together to calculate the total rate, Σr_i, which is substituted into Eq. (3) to determine the time step at which the next possible event occurs

$$\Delta t_v = \frac{-\ln(RN)}{\sum_i r_i} \tag{3}$$

where Δt_v defines the variable time step for the next event to occur and RN is a random number chosen between 0 and 1. A second random number is then chosen and used to determine which specific event occurs within the chosen time step by comparing the chosen number with the cumulative reaction probability distribution, as defined in Eq. (4)

$$P_i = \frac{r_i}{\sum_i r_i} \tag{4}$$

The reaction simulation proceeds in an event-by-event sequence whereby the time and the surface structure are updated at each time step. The simulation explicitly tracks all the molecular transformations together with the surface sites and as such can be used to the examine the influence of surface structure, alloy composition and spatial arrangement as well as reaction conditions on the detailed molecular product formation, the explicit surface coverages and the site preferences. This allows for the determination of these microscopic properties as well as the macroscopic properties which include the turnover frequencies (TOFs), apparent activation energies, reaction rates, and reaction orders.

We examined the kinetics for the selective hydrogenation of acetylene–ethylene mixtures over the well-defined Pd(1 1 1) and $Pd_{50\%}Ag_{50\%}$/Pd(1 1 1) surfaces in the temperature range of 298–378 K. The partial pressures of acetylene and ethylene were initially set at 0.37 kPa and 12.23 kPa, respectively, in order to mimic the industrial tail-end feedstock mixtures. As such, the acetylene concentration was fixed at 2.85%. The hydrogen partial pressure in the gas phase was varied from 0.37 kPa to 2.93 kPa to determine the effect of hydrogen pressures on the kinetics.

Each simulation was initialized by exposing the clean Pd(1 1 1) or $Pd_{50\%}Ag_{50\%}$/Pd(1 1 1) surfaces to the gas phase acetylene, ethylene, and hydrogen mixture. The simulations were run until the surface coverages as well as the turnover frequencies achieved steady state for over a period of 0.5–1.5 s. The acetylene conversion, as well as ethylene and ethane formation rates was calculated by plotting the number of molecules consumed (or formed) as a function of time and dividing the resulting slope of this graph by the number of sites to provide turnover frequencies. The surface coverages of the reaction intermediates reported herein were determined by averaging the instantaneous coverages over the full steady-state period. Since ethane was not allowed to re-adsorb in the simulation, the ethane formation rate was calculated by simply counting the number of ethane molecules that desorb from the surface as a function of time. The rate of ethylene formation was calculated as the difference between the rate of desorption and adsorption of ethylene. Similarly, the acetylene conversion rate was calculated by counting the net number of acetylene molecules consumed as a function of time and used as a measure of the reaction activity. The selectivity to ethylene production was defined as:

$$S_{C_2H_4} = 1 - \frac{r_{\text{ethane formation}}}{(-r_{\text{acetylene conversion}})} \tag{5}$$

where $r_{\text{ethane formation}}$ is the ethane formation rate; and $r_{\text{acetylene conversion}}$ is the acetylene conversion rate. Eq. (5) was used to determine the selectivity to avoid any difficulties in direct following the ethylene formation rate due to the statistical uncertainties in tracking the large number of ethylene re-adsorption and desorption events that occur in the simulation. A similar approach is also used in analyzing the experimental kinetics of tail-end mixture studies [7,8]. All the reported surface coverages were normalized based on the total number of surface atoms.

3. Results and discussion

3.1. Pd(1 1 1)

The kinetics for the selective hydrogenation of the acetylene–ethylene mixtures were first examined over the pure Pd(1 1 1) surface for partial pressures of hydrogen, acetylene, and ethylene of 0.74 kPa, 0.37 kPa, and 12.23 kPa, respectively. As shown in Fig. 3, the acetylene turnover frequency increases with increasing temperature. The apparent activation energy (44 kJ/mol) was determined by fitting the logarithm of acetylene turnover frequency with respect to the reciprocal of temperature in a classical Arrhenius expression. The simulated apparent activation energy was found to agree quite well with kinetic experiments carried out at low hydrogen partial pressure conditions (tail-end mixtures)

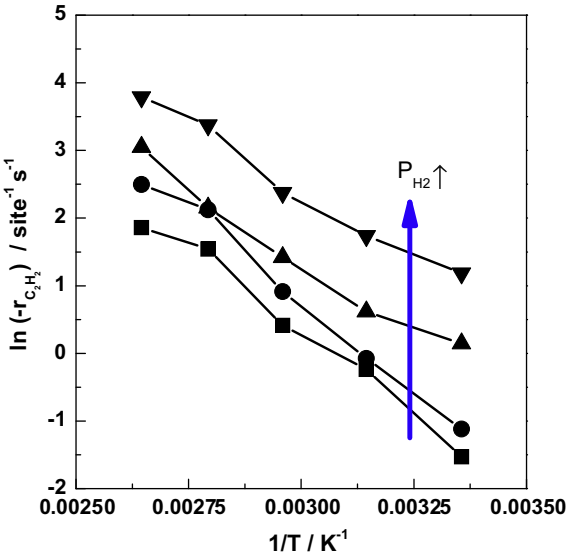

Fig. 3. The dependence of the acetylene turnover frequency (the rate of acetylene molecules converted per total number of sites per time) on the reaction temperature and hydrogen pressure for constant acetylene and ethylene pressures of $P_{C_2H_2} = 0.37$ kPa and $P_{C_2H_2} = 12.23$ kPa on Pd(1 1 1). (■) $P_{H_2} = 0.37$ kPa; (●) $P_{H_2} = 0.73$ kPa; (▲) $P_{H_2} = 1.47$ kPa; (▼) $P_{H_2} = 2.93$ kPa.

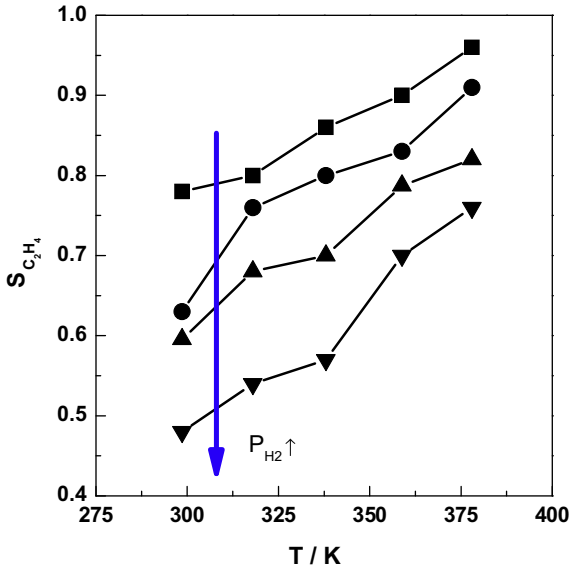

Fig. 4. The dependence of ethylene selectivity on the reaction temperature and hydrogen pressure for constant acetylene and ethylene pressures of $P_{C_2H_2} = 0.37$ kPa and $P_{C_2H_4} = 12.23$ kPa, respectively, on Pd(1 1 1). (■) $P_{H_2} = 0.37$ kPa; (●) $P_{H_2} = 0.73$ kPa; (▲) $P_{H_2} = 1.47$ kPa; (▼) $P_{H_2} = 2.93$ kPa.

in an industrial reactor (40 kJ/mol) [3]. The simulated apparent activation energy also agrees quite well with both experiments and simulations carried out for pure acetylene over the Pd(1 1 1) single crystal surface [42]. In addition, the turnover frequencies for the simulations for the hydrogenation of pure acetylene feeds were found to be in remarkably good agreement with those reported by Molero [42]. Experiments carried out at higher partial pressures of hydrogen, however, report apparent activation energies that are somewhat higher (59–71 kJ/mol) [5,6,12,13,74]. The composition of the reactant gas mixtures as well as the nature of the catalyst supports, however, is known to significantly influence the measured apparent activation energy [7]. For example, the apparent activation energies of 49 kJ/mol and 65 kJ/mol were found for the hydrogenation of a tail-end acetylene–ethylene mixture ($H_2/C_2H_2 = 2$), over Pd/Al_2O_3 and Pd/SiO_2, respectively, whereas a surprisingly high barrier of 106 kJ/mol was reported for the hydrogenation of a front-end mixture with a H_2/C_2H_2 ratio of 130 [7].

The simulated ethylene selectivities were found to increase with increasing temperature as is shown in Fig. 4. This is in agreement with our previous simulation results for pure acetylene hydrogenation over the Pd(1 1 1) surface [48]. The ethylene selectivity shown in Fig. 4 increased from 63% to 91% as the temperature increased from 298 K to 378 K. Higher temperatures increased the desorption of both ethylene and hydrogen which lowered their surface coverages and thus significantly decreased the rate of ethylene hydrogenation. The intrinsic activation barrier for the hydrogenation of ethylene (+72 kJ/mol) is only slightly lower than that for the desorption of ethylene (+82 kJ/mol) thus higher temperatures tend to readily promote ethylene desorption, lower the surface coverages of ethylene and hydrogen, and minimize the hydrogenation of ethylene.

The increased ethylene selectivity can also be rationalized in terms of mechanistic factors that control the hydrogen surface coverage. DFT results indicate that the intrinsic activation barrier for vinyl hydrogenation to ethylidene is 85 kJ/mol, which is higher than the barrier of 74 kJ/mol for selective path for vinyl hydrogenation to ethylene. As the temperature is increased, there is an increased desorption rate of hydrogen which limits the surface hydrogen atoms available to react with ethylene and shuts down the primary hydrogenation route to ethane. The parallel path to ethane formation which proceeds through the hydrogenation of vinyl to ethylidene followed by ethylidene to ethane is also shut down as a result of the limited surface hydrogen. The higher temperatures and the limited surface hydrogen concentrations instead selectively promote the dehydrogenation of ethylidene to ethylidyne over the hydrogenation to ethane. The simulations reveal that nearly all of the ethylidene reacts to form ethylidyne as the temperature is increased above 323 K. The ethylidyne that forms on the Pd(1 1 1) surface is fairly unreactive and tends to block the 3-fold fcc sites. This inhibits the hydrogen adsorption and as a result lowers the steady-state hydrogen coverage significantly which acts to prevent the unselective hydrogenation of ethylene to ethane. Consequently, the ethylene selectivity increases with the temperature.

As was discussed earlier, the hydrogenation of acetylene to ethylene is governed by the intrinsic activation barriers for the elementary hydrogenation steps as well as the steady-state surface coverages. We have therefore closely monitored the coverage for each of the reaction intermediates as a function of reaction conditions. The average surface coverages for the most abundant surface intermediates (acetylene, hydrogen, vinyl, and ethylidyne) are shown as a function of temperature in Fig. 5. The steady-state coverages of ethylene, ethyl, and ethylidene were all found to be less than 1%. The surface coverages were calculated as the number of adsorbates on the surface per surface Pd atom averaged over the entire steady-state time interval. The results in Fig. 5a show that the vinyl coverage decreased while the ethylidyne coverage increased with increasing temperature. As the temperature increased, the hydrogenation of vinyl to ethylene increased. The increased temperature, however, also increased the rate of ethylidene formation which readily dehydrogenates to form ethylidyne as was discussed above. The ethylidyne surface coverage therefore increased from 0.048 ML to 0.167 ML as the temperature increased.

The hydrogen surface coverage was found to be very low at all temperatures examined and decreased slightly from 0.004 ML at 298 K to 0.002 ML at 378 K as is shown in Fig. 5b. This decrease in hydrogen coverage at higher temperature is the result of its enhanced desorption. The decrease in the hydrogen surface coverage

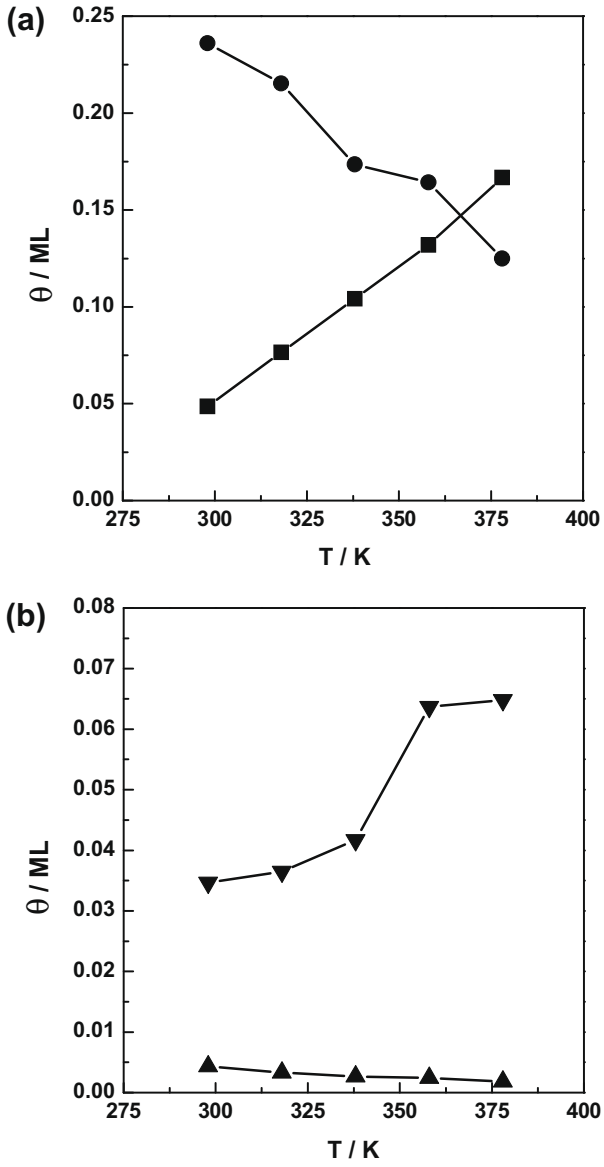

Fig. 5. The dependence of surface coverages on temperature over the Pd(1 1 1) surface at partial pressures of $P_{H_2} = 0.37$ kPa, $P_{C_2H_2} = 0.37$ kPa, $P_{C_2H_2} = 12.23$ kPa. (a) (●) vinyl; (■) ethylidyne; (b) (▼) acetylene; (▲) hydrogen.

is the result of the loss of vacant sites for H_2 dissociation due to an increase in the overall hydrocarbon surface coverage. This decrease in the surface coverage of hydrogen lowers the hydrogenation rates. As a result, this increases the acetylene surface coverage from 0.035 ML to 0.065 ML. The total surface coverage of all other minor carbonaceous intermediates such as C, CH, CH_2, and CH_3 was found to be less than 0.05% of the surface sites. The temperature dependence of the surface coverages of ethylene, ethylidene, and ethyl was not analyzed in this work since the calculated coverages were too low to be statistically significant. The simulations, for example, revealed that any ethylene that forms on the surface is either hydrogenated to ethane or rapidly desorbs from the surface. As the temperature increases, ethylene removal occurs predominantly through its desorption from the surface.

An important conclusion that can be drawn from the coverage results reported in Fig. 5 is that the Pd(1 1 1) surface is covered with vinyl, ethylidyne, and acetylene which result in overall surface coverages of about 0.35 ML. As these are C_2 species, they tend to block more than a single Pd site and as such inhibit the dissociative adsorption of hydrogen and thus limit the hydrogen surface coverage. The results are consistent with the ideas presented by Molnár et al. [75] who suggested that the surface is covered with hydrocarbon intermediates which can block H_2 activation and limit the hydrogen surface coverage. The hydrogen that dissociates on the surface readily reacts with acetylene or other neighboring hydrocarbons. This is consistent with the negative reaction order found for acetylene as it inhibits the surface and the first-order behavior for hydrogen.

The results discussed here can be compared with our previous simulation study for the hydrogenation of acetylene over Pd [48]. There are two key differences between these two studies. The first involves the differences in the initial composition of the feed. The previous study examined the hydrogenation of a pure acetylene feed, whereas the feed in the present work contains only 2.85% acetylene. The remaining fraction of the feed is ethylene which can co-adsorb and react with surface hydrogen. The second difference involves the increased number of reaction paths simulated in the present work. In the previous study, we examined only the selective hydrogenation of acetylene in the primary route. The present work provides a more extensive set of dehydrogenation pathways for both acetylene and ethylene. The latter difference results in a change in the most abundant surface intermediate from acetylene (found previously) [48] to vinyl and ethylidyne (found here).

The simulation results here demonstrate a significant increase in the ethylidyne surface coverage with the increasing temperature. The ethylidyne that forms is unreactive as the intrinsic activation barriers for its hydrogenation, dehydrogenation, and decomposition are quite high. It is strongly bound to the surface and thus blocks available surface sites needed for the activation of H_2 which limits the amount of hydrogen on the surface. This is consistent with experimental observations by Beebe et al. who showed the evolution of significant ethylidyne surface coverages in the selective hydrogenation of an acetylene–ethylene mixture over a Pd/Al_2O_3 catalyst [76]. Ethylidyne remained on the Pd surface up to 400 K without decomposing into C_1 fragments. At low partial pressures of hydrogen and high temperatures, ethylidyne accumulates and eventually poisons the surface by shutting down the dissociative adsorption of hydrogen [77]. At higher hydrogen partial pressures, ethylidyne is present but is quite mobile and thought to simply be a spectator species [41,77]. Simulations carried out at higher partial pressures of hydrogen as reported below show similar trends.

3.2. Pd–Ag/Pd(1 1 1)

Alloying Pd with Ag substantially increases the selectivity of Pd in the selective hydrogenation of acetylene [29–36]. In order to begin to elucidate the influence of Ag on the selective hydrogenation of acetylene, we carried out simulations over the two different model $Pd_{50\%}Ag_{50\%}$ alloy surfaces presented in Fig. 2. The first surface shown in Fig. 2b involves a uniformly dispersed Pd–Ag monolayer alloy on a Pd(1 1 1) substrate ($Pd_{50\%}Ag_{50\%}$/Pd(1 1 1)-dispersed) which contains bridging and atop Pd and Ag sites only. The 3-fold Pd sites are not present. The surface is consistent with those suggested by Jin et al. [32]. The second surface shown in Fig. 2c involves the formation of small alternating Pd_3 and Ag_3 ensembles which contain atop, bridging as well as 3-fold Pd and Ag sites. The steady-state activities and selectivities as well as a detailed breakdown of the surface coverages at different temperatures and partial pressures over these two $Pd_{50\%}Ag_{50\%}$ alloys are compared with one another as well as with the results over the pure Pd(1 1 1) substrate in order to analyze both the geometric (ensemble) and ligand (electronic) effects that occur upon alloying.

The simulations on the $Pd_{50\%}Ag_{50\%}$ alloys were carried out at the same conditions used in the simulations over the Pd(1 1 1) surface.

Results comparing the two different alloys with pure Pd surface are presented in Figs. 6 and 7. The simulated acetylene turnover frequencies over these two different alloy surface ensembles plotted as a function of temperature in Fig. 6 are quite similar with the calculated apparent activation energies of 36 kJ/mol for the $Pd_{50\%}Ag_{50\%}$-dispersed alloy and 38 kJ/mol for the $Pd_{50\%}Ag_{50\%}$-ensemble alloy. The ethylene selectivities for these two alloy surfaces which are shown in Fig. 7 are also nearly identical over the full range of temperatures examined. The results suggest that there is little influence in the arrangement of the atomic surface structure of the alloys on the kinetics or the selectivities for acetylene hydrogenation over the $Pd_{50\%}Ag_{50\%}$/Pd(1 1 1) surfaces. Since the effects of the actual alloy structure were found to be negligible, we carried out the remaining simulations only over the uniformly dispersed $Pd_{50\%}Ag_{50\%}$/Pd(1 1 1) surface. The insensitivity to the surface alloy configuration in the simulations is not consistent with the experimental results by Jin et al. [32] who suggested that the selective hydrogenation of front-end acetylene–ethylene feeds can vary depending upon the specific surface alloy configuration that is present. The difference may be due to the different feedstocks considered. Jin et al. suggested that the higher activity of the dispersed alloy is due to its ability to shut down the larger Pd ensembles responsible for the significant oligomerization than those results from hydrogenating tail-end feeds [32]. The simulations results reported herein, however, were carried out over a front-end feed which has considerably greater hydrogen partial pressures than the tail-end feed and thus undergoes very little oligomerization. As such these oligomerization paths were also not considered here.

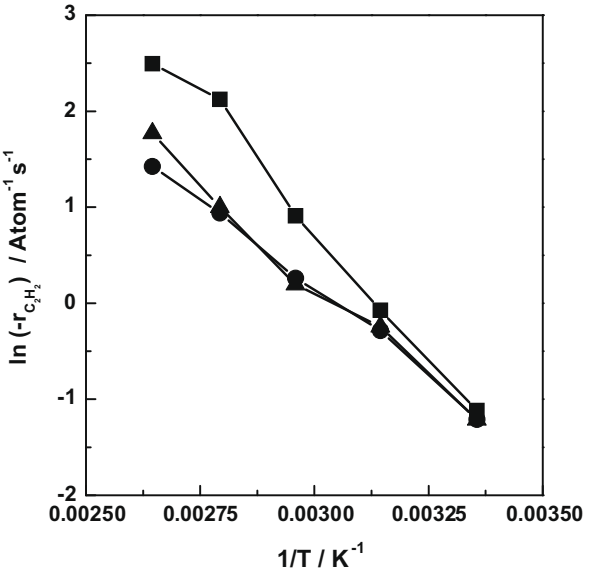

Fig. 6. Comparison of the acetylene turnover frequencies at partial pressures of $P_{C_2H_2} = 0.37$ kPa; $P_{C_2H_2} = 12.23$ kPa and $P_{H_2} = 0.73$ kPa over the Pd(1 1 1) and the $Pd_{50\%}Ag_{50\%}$/Pd(1 1 1) alloy surfaces. (■) Pd(1 1 1) surface (●) uniformly dispersed $Pd_{50\%}Ag_{50\%}$/Pd(1 1 1) surface; (▲) triangular ensemble $Pd_{50\%}Ag_{50\%}$/Pd(1 1 1) surface.

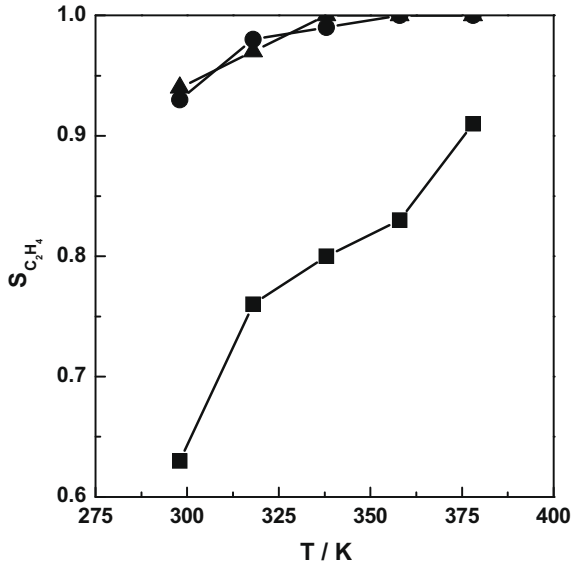

Fig. 7. Comparison of the ethylene selectivity at partial pressures of $P_{C_2H_2} = 0.37$ kPa; $P_{C_2H_2} = 12.23$ kPa and $P_{H_2} = 0.73$ kPa over the Pd(1 1 1) and the $Pd_{50\%}Ag_{50\%}$/Pd(1 1 1) alloy surfaces. (■) Pd(1 1 1) surface (●) uniformly dispersed $Pd_{50\%}Ag_{50\%}$/Pd(1 1 1) surface; (▲) triangular ensemble $Pd_{50\%}Ag_{50\%}$/Pd(1 1 1) surface.

Significant differences can be seen in comparing the kinetics over pure Pd with that over the Pd–Ag alloy. The results depicted in Fig. 6 show a decrease in the acetylene turnover frequency as Ag is alloyed in the surface over a temperature range of 298–378 K. The rate of acetylene conversion decreased over the $Pd_{50\%}Ag_{50\%}$/Pd(1 1 1) surface. This is consistent with the results from temperature-programed reaction studies under UHV conditions as well as actual reaction studies which suggest that the overall rate is slightly decreased upon alloying Ag into the Pd [33]. The apparent activation energy for the selective hydrogenation of acetylene over the $Pd_{50\%}Ag_{50\%}$-dispersed surface obtained from an Arrhenius relationship was calculated to be 36 kJ/mol, which is slightly lower than the value of 44 kJ/mol found for the Pd(1 1 1) surface. This indicates that while the rate per total number of metal sites decreases the rate per actual Pd is slightly more reactive, especially at low temperatures. The turnover frequencies reported in the literature are given on a per total site basis. The results reported here suggest that the rate on a per Pd site basis might increase slightly.

The apparent activation energies found here are over 20 kJ/mol lower than the DFT intrinsic activation barriers. The differences may be the result of the inclusion of adsorption energies in the simulations of the apparent activation barriers or due to lateral repulsive interactions between surface adsorbates. The calculated kinetics however clearly reveal that these simple rate models which ignore interactions between adsorbates cannot appropriately capture the chemistry and as such require the introduction of special sites and empirical fitting. The fact that acetylene has a non-integral order of −0.5 experimentally and −0.4 herein reveals that lateral interactions between the adsorbates are clearly playing a role. As such, one cannot use a simple rate expression to determine the interplay between the intrinsic activation barriers and adsorption constants for acetylene and hydrogen. DFT calculations carried out at higher surface coverages show a decrease of 46 kJ/mol as the coverage of the alkene or alkyne is increased. [5] This decrease, which is the direct result of the lateral repulsive interactions between adsorbates, is consistent with the changes reported here for the intrinsic and apparent activation barrier. We therefore suspect that the lower apparent activation barrier obtained in this work arises largely from the repulsive interaction between adsorbates but cannot establish how much of this is due to the differences that result from the inclusion of adsorption energies in the simulations.

The simulations presented in Fig. 7 show a significant increase in the ethylene selectivity over the $Pd_{50\%}Ag_{50\%}$/Pd(1 1 1) surface in comparison with that over pure Pd, especially at lower temperatures. The ethylene selectivity was found to be over 93% on the $Pd_{50\%}Ag_{50\%}$/Pd(1 1 1) surface and only 62% over the pure Pd(1 1 1) surface at 298 K. As the temperature was increased to 378 K, the

ethylene selectivity increased from 93% to 99.5% over the alloy while that on the pure Pd increased from 62% to 90%. This is consistent with the experimental results which show that alloying Ag increases the ethylene selectivity [33,36,40,78].

The surface coverages of the reaction intermediates that form on the $Pd_{50\%}Ag_{50\%}$/Pd(1 1 1) surface shown in Fig. 12 were found to be rather different from those that result on the Pd(1 1 1) surface. The results indicate that the dehydrogenation as well as the C–C bond-breaking paths which require larger surface ensembles are effectively shut down on the $Pd_{50\%}Ag_{50\%}$/Pd(1 1 1) surface. The unselective hydrogenation paths that lead to ethylidyne and ethane were also significantly inhibited as a result of the presence of Ag in the surface. The results show that the selective hydrogenation of acetylene over the $Pd_{50\%}Ag_{50\%}$/Pd(1 1 1) surface predominantly follows the very simple sequence of consecutive hydrogen addition steps shown along the second row in Fig. 1. There is very little formation of ethylidyne, ethylidene, or C_1 intermediates.

Acetylene was found to be the most abundant intermediate on the $Pd_{50\%}Ag_{50\%}$/Pd(1 1 1) surface which is in sharp contrast to the results found over the pure Pd surface, which show that vinyl or ethylidyne cover the surface. The surface coverage of acetylene was found to increase with increasing temperature over the $Pd_{50\%}Ag_{50\%}$/Pd(1 1 1) surface. At 298 K, for example, the acetylene coverage was found to be 0.14 ML, whereas at 378 K the acetylene coverage increased to 0.24 ML.

The vinyl intermediate that forms as a result of the hydrogenation of acetylene was found to be less than 0.02 ML on the $Pd_{50\%}Ag_{50\%}$/Pd(1 1 1) surface for all the reaction conditions examined. This is significantly lower than the surface coverage of vinyl on Pd(1 1 1) which ranged from 0.12 to 0.23 ML. This drop in the vinyl surface coverage is the result of the significant increase in the rate of vinyl hydrogenation over the $Pd_{50\%}Ag_{50\%}$/Pd(1 1 1) surface. Any vinyl that forms is very rapidly hydrogenated to ethylene over the alloy surface. This is in contrast to the slower rates of hydrogenation of vinyl to ethylene over pure Pd. The contrasting difference in the rate of vinyl hydrogenation over the pure Pd surface and the $Pd_{50\%}Ag_{50\%}$/Pd(1 1 1) surface is attributed to the significant decrease (64 kJ/mol) in the activation barrier for the hydrogenation of vinyl that results upon alloying Pd with Ag. While this reduction is due to both ensemble and electronic effects, the ensemble effect is the more predominant of the two as the $Pd_{50\%}Ag_{50\%}$/Pd(1 1 1) surface used here is devoid of the 3-fold Pd sites which stabilize the binding of vinyl on Pd. The adsorption of the vinyl intermediate therefore drops by over 60 kJ/mol in moving from the pure Pd to the $Pd_{50\%}Ag_{50\%}$/Pd(1 1 1) surface.

The simulations show that the unselective hydrogenation of vinyl to ethylidene which was found to be competitive with the hydrogenation of vinyl to ethylene over the pure Pd surface is effectively shut down over the $Pd_{50\%}Ag_{50\%}$/Pd(1 1 1) surface. The enhanced rate for the hydrogenation of vinyl to ethylene ultimately prevents vinyl from reacting via the slower channel to form ethylidyne. The presence of Ag prevents the formation of the 3-fold Pd ensembles which forces the vinyl intermediate to bind in an η_1 configuration solely through the CH group. The CH_2 end of vinyl intermediate is pushed from the surface thus inhibiting hydrogenation addition to form ethylidyne. The loss of the larger Pd ensembles on the $Pd_{50\%}Ag_{50\%}$/Pd(1 1 1) surface also effectively shuts down the C–C bond-breaking steps and thus prevents the unselective paths that lead to the formation of C_1 intermediates.

The simulations reveal that very little ethane is formed over the $Pd_{50\%}Ag_{50\%}$/Pd(1 1 1) surface. This is predominantly due to the fact that the Ag significantly weakens the adsorption of ethylene which allows it to readily desorb from the surface before it can ever react. The reduction in the binding energies of both vinyl and acetylene on the $Pd_{50\%}Ag_{50\%}$/Pd(1 1 1) surface enhances their hydrogenation

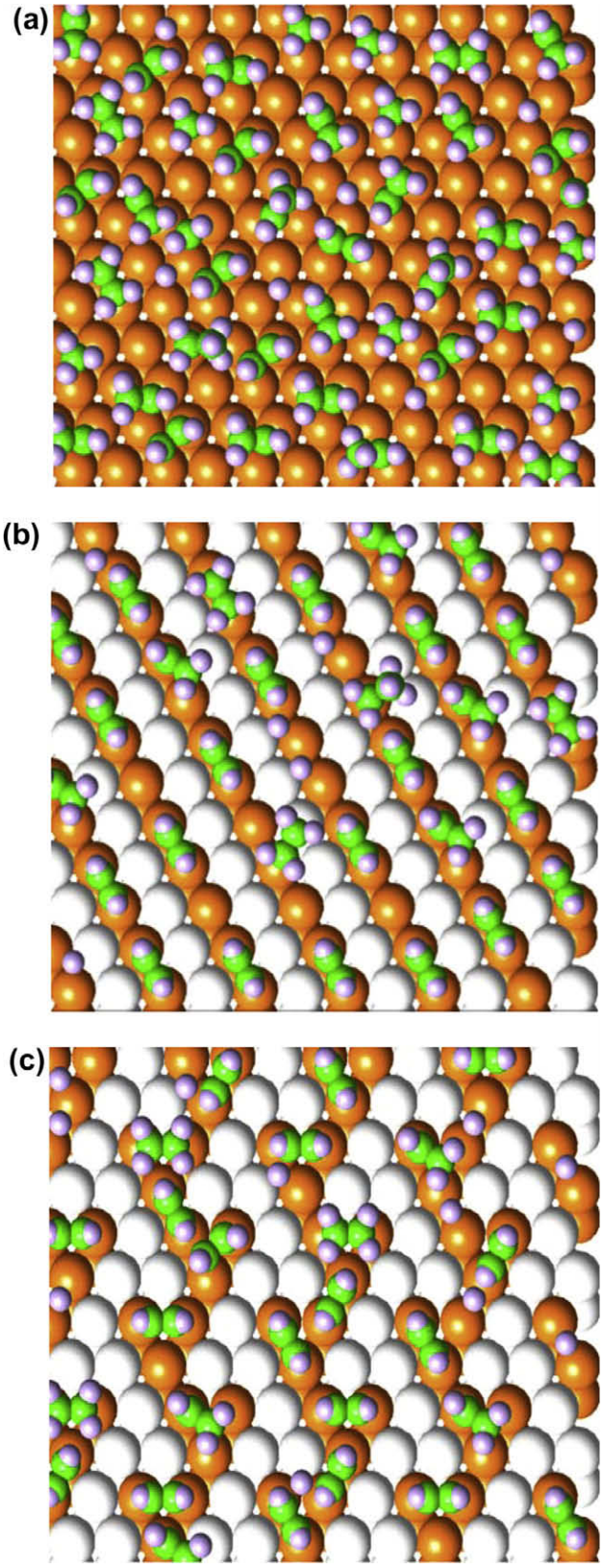

Fig. 8. Snapshots of the surfaces from simulations. (a) Pd(1 1 1) surface; (b) uniformly dispersed $Pd_{50\%}Ag_{50\%}$/Pd(1 1 1) surface; (c) triangular ensemble $Pd_{50\%}Ag_{50\%}$/Pd(1 1 1) surface. The orange spheres and the white spheres represent Pd and Ag atoms, respectively. The C and H atoms are in green and gray, respectively. (For interpretation of the references to colour in this figure legend, the reader is referred to the web version of this article.)

rates. The weaker adsorption of ethylene, however, decreases its rate of hydrogenation and promotes its desorption before it can react to form ethyl or ethane. Desorption is the predominant channel and as such strongly contributes to the very highly selectivities found over the alloy surface.

The kinetic Monte Carlo simulations allow us to track the microscopic details involved in the molecular transformations that occur over the metal surface and thus give rise to the macroscopic kinetic behavior. Knowledge of adsorption sites as well as the adsorbate orientations on the surface at steady-state conditions was useful to establishing the dominant reaction pathways that control the selective hydrogenation of acetylene over both the Pd(1 1 1) and the $Pd_{50\%}Ag_{50\%}$/Pd(1 1 1) surfaces.

A typical snapshot of the Pd(1 1 1) adlayer structure is shown in Fig. 8a. The Pd(1 1 1) surface is dominated by vinyl, ethylidyne, and acetylene. All three of these intermediates are strongly held to the surface and prefer the 3-fold Pd coordination sites. They therefore limit the dissociative adsorption of hydrogen and as such control the hydrogen surface coverage. The ethylene that forms binds at either bridging Pd sites (di-σ) or atop of Pd (π-bound). It is hydrogenated further to form an ethyl intermediate which binds atop of Pd and ethane which desorbs for the surface.

Fig. 8b depicts a snapshot of the steady-state adlayer on the $Pd_{50\%}Ag_{50\%}$/Pd(1 1 1) surface with a uniform Ag distribution. It is clear from these figures that the presence of Ag in the surface significantly changes the adlayer coverage and composition. As discussed earlier, the addition of Ag leads to a loss of the 3-fold Pd ensembles. This forces acetylene to move from its stable η_1–η_2 adsorption site to a bridging Pd site where it is held much more weakly. Acetylene is thus hydrogenated more readily to form vinyl. The vinyl intermediate also shifts from its most favorable η_1–η_2 Pd adsorption site to an atop Pd site on the $Pd_{50\%}Ag_{50\%}$/Pd(1 1 1) surface. Both hydrogen and ethylene were less discriminatory and maintained their 3-fold (Pd–Pd–Ag) and the bridge (Pd–Pd) sites, respectively. Fig. 8c shows a snapshot of the adlayer structure at steady-state conditions over the Pd_3–Ag_3 ensemble $Pd_{50\%}Ag_{50\%}$/Pd(1 1 1) surface. A similar adlayer structure appears to form as that on the dispersed $Pd_{50\%}Ag_{50\%}$/Pd(1 1 1) surface which helps to explain the similarities in the activity and selectivity discussed earlier for these two Pd–Ag alloy surfaces.

3.3. The effect of hydrogen pressure

The effect of hydrogen on the kinetics for the selective hydrogenation of acetylene over the Pd(1 1 1) as well as the dispersed $Pd_{50\%}Ag_{50\%}$/Pd(1 1 1) surfaces was examined by varying the partial pressure of hydrogen from 0.37 kPa to 2.93 kPa for different temperatures. The acetylene turnover frequency increased with increasing hydrogen partial pressure over both surfaces as a function of temperature as is shown in Figs. 3 and 9. The apparent activation energy for acetylene hydrogenation over the pure Pd surface dropped slightly from 44 to 32 kJ/mol as the hydrogen pressure was increased from 0.74 to 2.93 kPa. This indicates that hydrogenation increases with increasing hydrogen coverage. Duca et al. studied the kinetics of acetylene–ethylene mixtures over Pd/pumice catalysts in a continuous flow fixed-bed microreactor at atmospheric pressure over a temperature range of 283–340 K [8]. They showed a similar decrease in the apparent activation energy with the increasing ratio of $P_{H_2}/P_{C_2H_2}$. The decrease, however, was significantly larger with a reduction in the apparent barrier from 58 to 36 kJ/mol as the ratio of $P_{H_2}/P_{C_2H_2}$ was increased from 45 to 130 [8]. The simulation results for the $Pd_{50\%}Ag_{50\%}$/Pd(1 1 1) alloy presented in Fig. 9 reveal that there is a very slight decrease (4 kJ/mol) in the activation barrier with increasing hydrogen partial pressure. The differences are, however, very small and may be within the statistical precision of the simulations.

While there is little influence of the hydrogen partial pressure on the apparent activation barrier, the effect of hydrogen on ethylene selectivity is quite significant. The selectivity over the pure Pd(1 1 1) decreases with increasing the partial pressure of hydrogen. The results in Fig. 4 showed that as the hydrogen partial pressure is increased from 0.37 to 2.93 kPa, the ethylene selectivity decreased from 98% to 56% on the Pd(1 1 1) surface at 298 K, and from 78% to 48% at 378 K. This is consistent with the experimental measurements [8,40]. Duca et al., for example, showed a substantial increase in ethane production over supported Pd catalyst as the ratio of $P_{H_2}/P_{C_2H_2}$ increases from 2 to 130 [8]. Similarly, Bond et al. reported that the ethylene selectivity decreased from 96% to 87% at 295 K as the hydrogen partial pressure was increased from 100 mm Hg to 250 mm Hg for acetylene hydrogenation over Pd/α-Al_2O_3. The loss in selectivity at higher partial pressures of

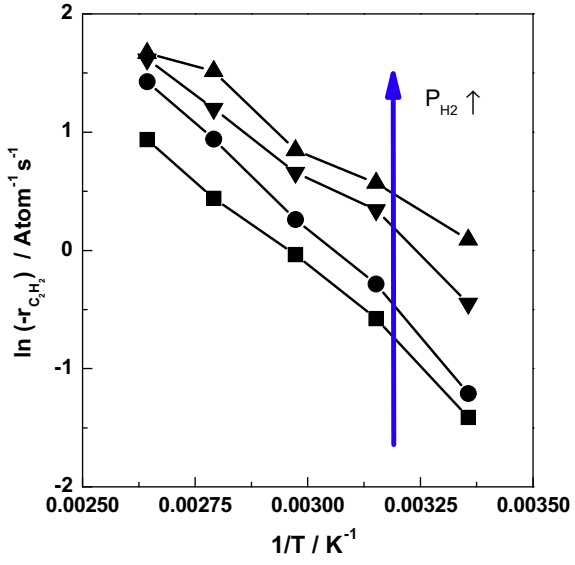

Fig. 9. The dependence of the acetylene turnover frequency on hydrogen partial pressure at different temperatures over the uniformly dispersed $Pd_{50\%}Ag_{50\%}$/Pd(1 1 1) alloy surface. (■) $P_{H_2} = 0.37$ kPa; (●) $P_{H_2} = 0.73$ kPa; (▲) $P_{H_2} = 1.47$ kPa; (▼) $P_{H_2} = 2.93$ kPa.

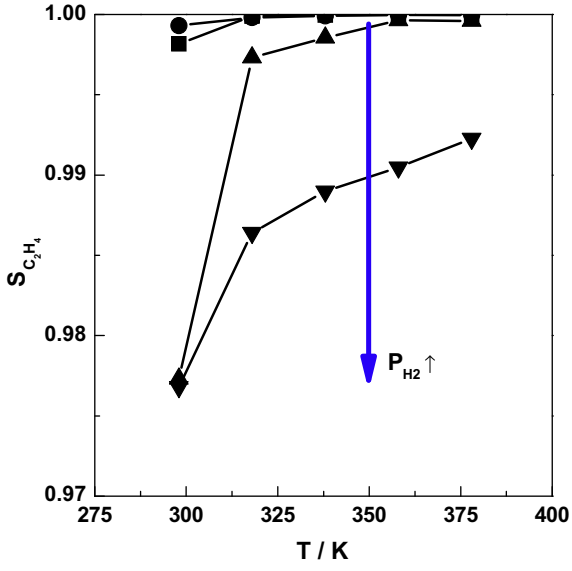

Fig. 10. The dependence of ethylene selectivity on hydrogen partial pressure at different temperatures over the uniformly dispersed $Pd_{50\%}Ag_{50\%}$/Pd(1 1 1) alloy surface. (■) $P_{H_2} = 0.37$ kPa; (●) $P_{H_2} = 0.73$ kPa; (▲) $P_{H_2} = 1.47$ kPa; (▼) $P_{H_2} = 2.93$ kPa.

hydrogen has also been suggested to be the result of the formation of the more active yet unselective β hydride phase of Pd [1,2]. The influence of hydrogen on selectivity was found to be significantly weaker over the $Pd_{50\%}Ag_{50\%}$/Pd(1 1 1) surface. Fig. 10, for example, indicates that the ethylene selectivity decreased by only 2% (from 99.8% to 97.7%) at 298 K as hydrogen partial pressure increased from 0.37 to 2.93 kPa. This is comparable to experimentally measured ethylene selectivity that decreases from 99% to 95% at 294 K for Pd–Ag alloy with 10% Ag [40]. Alloying Ag allows the catalytic surface to become much more resilient to the increased hydrogen pressures. This is also consistent with the experimental results from Khan et al. [33].

The simulations were used to determine the macroscopic reaction orders to further compare with experiment. The simulated acetylene turnover frequencies taken as a function of hydrogen acetylene and ethylene partial pressures were fit to Eq. (6) to establish the macroscopic reaction orders

$$-r_{C_2H_2}(\mathrm{TOF}) = \nu \cdot \exp\left(-\frac{E_a}{RT}\right) P^x_{C_2H_4} \cdot P^y_{C_2H_2} \cdot P^z_{H_2} \quad (6)$$

The hydrogen reaction order was found to increase from 1.1 to 1.3 over the Pd(1 1 1) surface as the temperature was increased from 318 K to 378 K. These orders are consistent with the experimental results which range from 1.0 to 1.5 over different supported Pd catalysts over different feed conditions [3,79].

The simulated hydrogen reaction order over the dispersed-$Pd_{50\%}Ag_{50\%}$/Pd(1 1 1) alloy was found to be just slightly higher than the pure Pd(1 1 1) surface which increased very weakly from 0.9 to 1.1 as the temperature was increased from 298 K to 378 K. The predicted hydrogen order is lower than the experimental order of 1.68 reported by Bond et al. for Pd–Ag (10 wt% Ag and 20 wt% Ag) alloy catalysts at 293 K [40].

The acetylene reaction orders were calculated to be −0.4 over the Pd(1 1 1) surface at 323 K and $P_{H_2} = 0.37$ kPa, $P_{C_2H_4} = 12.23$ kPa (Fig. S1 of Supplementary information). This is consistent with our previous simulations [48] and the experimental results reported by Molero [42] and −0.21 over $Pd_{50\%}Ag_{50\%}$/Pd(1 1 1) at the same conditions. Acetylene binds quite strongly to Pd and in addition leads to the formation of vinyl and ethylidyne. All these intermediates

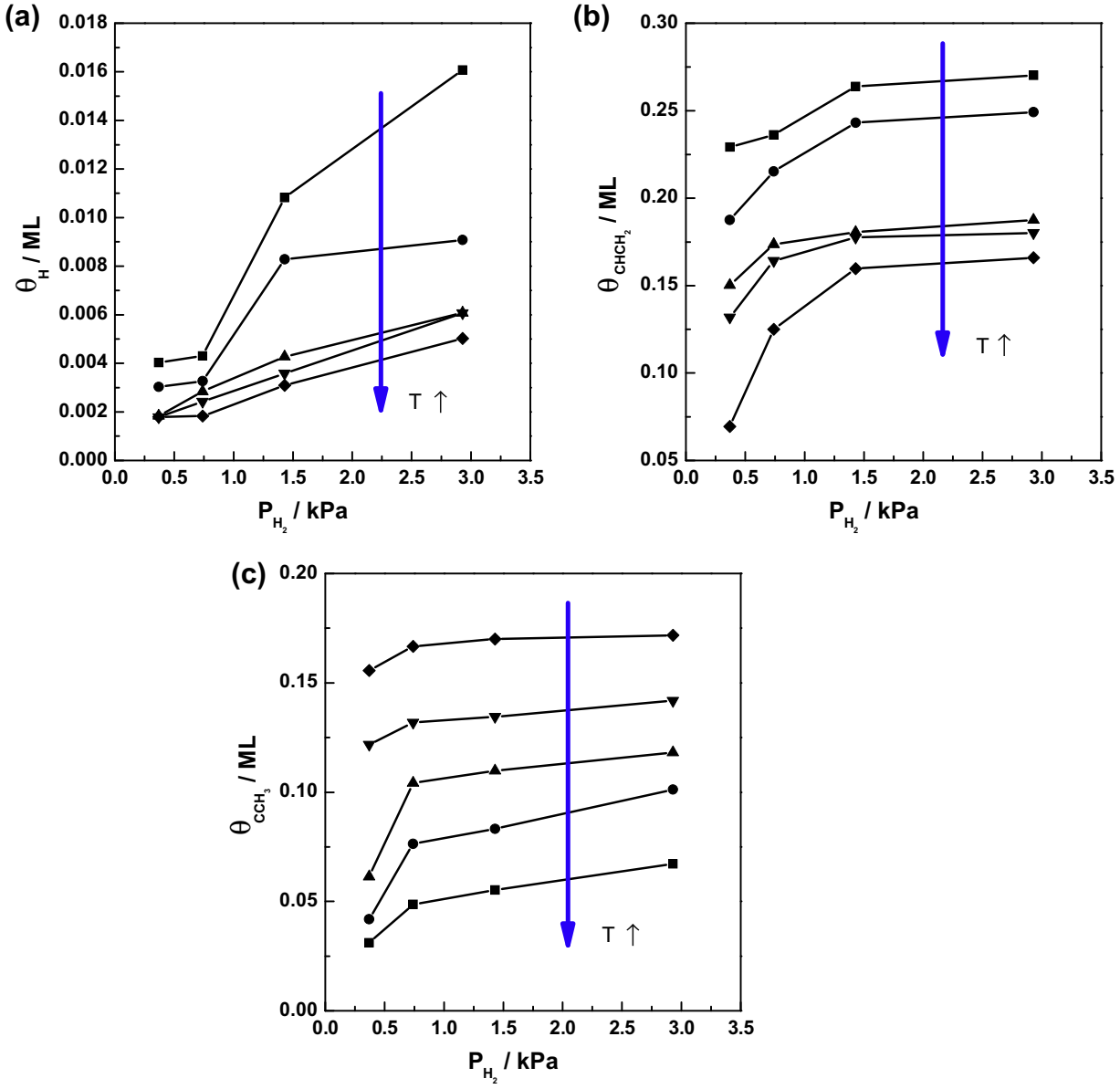

Fig. 11. The dependence of surface coverage on the hydrogen partial pressure over the Pd(1 1 1) surface. (a) Hydrogen; (b) vinyl; (c) ethylidyne. (■) $T = 298$ K; (●) $T = 323$ K; (▲) $T = 348$ K; (▼) $T = 373$ K; (♦) $T = 398$ K.

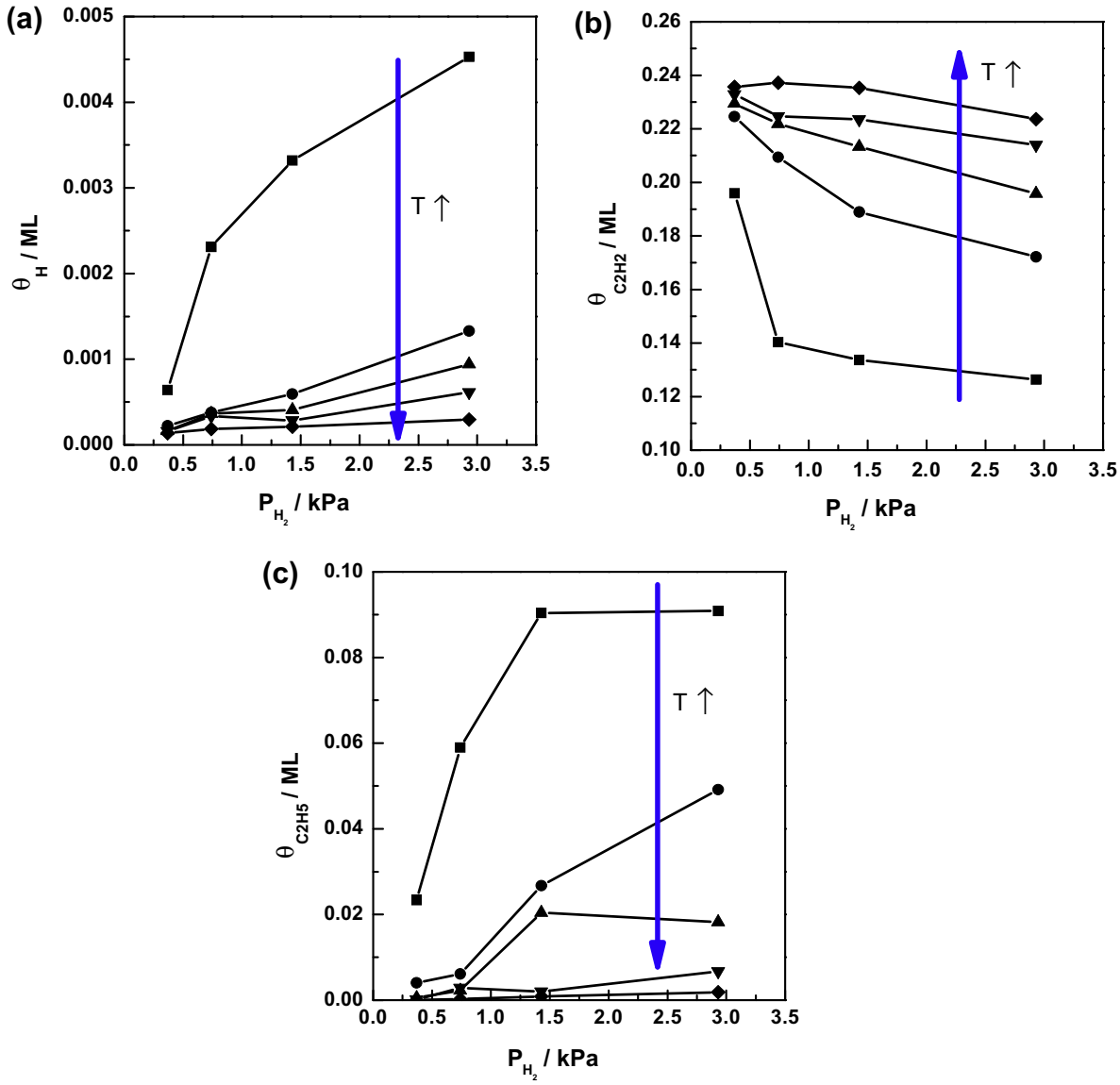

Fig. 12. The dependence of surface coverage on the hydrogen partial pressure over the uniformly dispersed $Pd_{50\%}Ag_{50\%}$/Pd(1 1 1) alloy surface. (a) Hydrogen; (b) acetylene; (c) ethyl. (■) T = 298 K; (●) T = 323 K; (▲) T = 348 K; (▼) T = 373 K; (♦) T = 398 K.

block the sites needed for the dissociation of hydrogen and as such result in negative reaction orders. The addition of Ag slightly weakens this effect but there is still a competition for site as the reaction order is −0.21.

The ethylene reaction orders on the Pd(1 1 1) and $Pd_{50\%}Ag_{50\%}$/Pd(1 1 1) surfaces were found to be +0.03 and −0.02, respectively (Fig. S1 of Supplementary information). Both are essentially zero order and there is very little change in moving to the Pd–Ag alloy.

The effect of the hydrogen partial pressure on the surface coverages of hydrogen, vinyl, and ethylidyne over Pd(1 1 1) is shown in Fig. 11. As might be expected, the hydrogen surface coverage increases with increases in the hydrogen partial pressure. This trend is more distinctive at lower temperatures. At 298 K, the hydrogen coverage increased from 0.004 to 0.016 ML as the hydrogen pressure was increased from 0.37 to 2.93 kPa. This increase in hydrogen surface coverage promotes the linear increase in the acetylene hydrogenation rates with hydrogen pressure. The higher hydrogen pressures, however, also promotes the hydrogenation of all the surface intermediates which results in the over-hydrogenation of ethylene and a significant loss in selectivity.

The effect of hydrogen partial pressure on the acetylene coverage was found to be rather weak. The influence on the vinyl coverage, however, was much more significant whereby increasing the hydrogen partial pressure increased the coverage of vinyl (Fig. 11b). The increase in vinyl coverage is the result of an increase in the rate of acetylene hydrogenation over Pd with hydrogen pressure. While there was only a slight increase in the ethylidyne coverage with an increase in the hydrogen partial pressure over Pd as shown in Fig. 11c, the hydrogenation of ethylidene to ethyl as well as the subsequent hydrogenation of ethyl to ethane became noticeable higher at the higher partial pressures of hydrogen. This is consistent with the ideas presented in [1,2,15,16] which suggest that there is a secondary path which leads to the hydrogenation of acetylene to ethane that does not have to proceed through ethylene but instead goes through ethylidene.

The effect of hydrogen partial pressure on the surface coverages for the most abundant surface intermediates in the selective hydrogenation of acetylene over the dispersed $Pd_{50\%}Ag_{50\%}$/Pd(1 1 1) surface is shown in Fig. 12. While the hydrogen coverage increased with the hydrogen pressure, the acetylene coverage

decreased. The higher hydrogen partial pressures increased the rate of acetylene hydrogenation which ultimately led to the decrease in the acetylene surface coverage. The increase in the partial pressures of hydrogen also increased the rate of ethylene and ethylidene hydrogenation which results in an increase in the coverage of ethyl intermediates as shown in Fig. 12c. Since the barriers for ethyl dissociation back to ethylene and ethylidene were only 41 and 58 kJ/mol, which are considerably lower than the barrier of ethyl hydrogenation to ethane (78 kJ/mol), very little ethane is actually formed. The selectivity to ethylene over the Pd–Ag alloys was therefore found to be much more resilient to changes in the pressures of hydrogen and changes in the overall operating conditions than the pure Pd surface was.

It is important to point out again that we not included the hydride or carbide formation which are known to form on Pd and can significantly influence the selectivity [1,2,21–23]. As such the simulations do not appropriately capture the decrease in selectivity that occurs at higher temperatures and higher hydrogen pressures due to the formation of the unselective β-hydride phase. In addition, the simulations do not include routes for the formation of carbide, coke, or oligomeric carbon all of which are known to occur on Pd at higher temperatures. The carbide phase is thought to be highly selective as it limits the formation of subsurface hydrogen [21–23]. While both hydride and carbide phases are clearly important for supported Pd, their formation and importance to the catalytic hydrogenation on the PdAg alloys, however, is unclear. We expect that the simulations reported herein should agree reasonably well with the experimental data at the lower temperatures and hydrogen pressures examined herein.

4. Summary/conclusions

A first-principles-based kinetic Monte Carlo simulation was constructed and used to follow the molecular transformations and the kinetics for the selective hydrogenation of acetylene from ethylene feedstocks over the pure Pd and the Pd–Ag alloy surfaces. The kinetics for the hydrogenation of acetylene was established from first-principles DFT calculations over the Pd and Pd–Ag alloy surfaces. The ab initio results were used together with a van der Waals model from the Merck Force Field and a BOC lateral interaction model to construct a kinetic database for a site-explicit variable time step kinetic Monte Carlo simulation used to follow the molecular transformations involved in the selective hydrogenation of a front-end acetylene–ethylene feed over the Pd(1 1 1) and bimetallic $Pd_{50\%}Ag_{50\%}$/Pd(1 1 1) surfaces. The simulations explicitly follow the elementary steps involved in the two parallel hydrogenation routes which proceed through the formation of ethylene and ethylidene, respectively, to form ethane. The simulations also followed the unselective C_2 dehydrogenation and the C–C bond-breaking paths.

The simulations reveal that the activity and the selectivity of acetylene hydrogenation are controlled by an optimal balance of hydrogen and ethylene on the surface. On the pure Pd(1 1 1) surface, the overall rate is governed by the dissociative adsorption of hydrogen onto the surface and the availability of hydrogen on the surface to carry out the hydrogenation steps. Vinyl, ethylidyne, and acetylene, which are the most abundant surface intermediates, cover up to 0.35 ML of the surface which blocks access to 3-fold coordination sites and inhibits the dissociative adsorption of hydrogen. Increasing the reaction temperature increased both the catalytic activity and the selectivity. The increase in the rate with temperature is due to the increase in the hydrogenation rate constant with temperature. The increase in the selectivity to ethylene with temperature is controlled by the increased rate of acetylene and vinyl hydrogenation together with the increased rate of ethylene desorption. The selectivity is also promoted by an increase in the rate of ethylidyne formation as a result of the concomitant increase in ratio of dehydrogenation to hydrogenation of ethylidene. Ethylidyne is a stable surface intermediate that ultimately leads to intermolecular repulsive interactions within the adlayer that enhance the hydrogenation of ethylene and vinyl intermediates, promote the desorption of ethylene, and prevent the C–C bond-breaking reactions as well as the over-hydrogenation to ethane. Increasing the partial pressure of hydrogen increases the acetylene turnover frequency as the reaction is first order in hydrogen. The increase in hydrogen partial pressure, however, also increases the availability of hydrogen on the surface which catalyzes the unselective hydrogenation paths that lead to the formation of ethane and the loss in the overall selectivity to ethylene.

Alloying the surface with Ag results in both ensemble and electronic effects which weaken the binding energies of acetylene and hydrogen to the surface. The presence of Ag in the surface weakens the binding strengths for all surface intermediates including acetylene, vinyl, hydrogen, and ethylene which increases their rates for desorption as well as their rates of hydrogenation. The weaker interactions and the loss of Pd sites control the availability of hydrogen on the surface. This, together with the weaker ethylene binding to the surface, promotes ethylene desorption over ethylene hydrogenation. This significantly improves the selectivity in the studied temperature range. The presence of Ag on the Pd(1 1 1) surface also shuts down the larger Pd ensembles which can lead to the C–C bond breaking as well as ethylidyne formation. While the overall rate of acetylene conversion decreases as a result of the decrease in the number of surface Pd atoms, there is a slight increase in turnover frequency on a per Pd site basis.

On both the pure Pd(1 1 1) and the $Pd_{50\%}Ag_{50\%}$/Pd(1 1 1) surfaces, the activity is controlled by weakening the bonding of acetylene and hydrogen to the surface. On Pd(1 1 1), this occurs via the presence of ethylidyne that forms during reaction, whereas on the $Pd_{50\%}Ag_{50\%}$/Pd(1 1 1) surface this occurs via the presence of Ag. The selectivity on both Pd and $Pd_{50\%}Ag_{50\%}$/Pd(1 1 1) surfaces is optimized by controlling the availability of hydrogen and by enhancing the rate of ethylene desorption over hydrogenation. On the Pd(1 1 1) surface this is governed by the steady-state ethylidyne surface coverage that forms as a result of reaction, whereas on the $Pd_{50\%}Ag_{50\%}$/Pd(1 1 1) surface it is the result of Ag on the surface. Ethylidyne which is formed during the reaction over Pd promotes the activity and the selectivity of the reaction via the same mechanisms as those of Ag. Its formation requires somewhat higher temperatures and it is slightly less effective than Ag. At higher temperatures, ethylidyne readily forms on the surface and helps to enhance the selectivity to ethylene.

Acknowledgments

The authors acknowledge Dow Chemical Company for financial support of this work. This work was also partially supported by a Laboratory Directed Research and Development (LDRD) project of the Pacific Northwest National Laboratory (PNNL). The authors also kindly acknowledge the computational resources used for calculating activation barriers for a number of the steps provided by the EMSL, a national scientific user facility sponsored by the Department of Energy's Office of Biological and Environmental Research and located at Pacific Northwest National Laboratory.

Appendix A. Supplementary data

Supplementary data associated with this article can be found, in the online version, at doi:10.1016/j.jcat.2009.09.004.

References

[1] A. Borodzinski, Catal. Rev.-Sci. Eng. 48 (2006) 91–144.
[2] A. Borodzinski, G.C. Bond, Catal. Rev.-Sci. Eng. 50 (2008) 379–469.
[3] A.N.R. Bos, E.S. Bootsma, F. Foeth, H.W.J. Sleyster, K.R. Westerterp, Chem. Eng. Process. 32 (1993) 53–63.
[4] A.N.R. Bos, K.R. Westerterp, Chem. Eng. Process. 32 (1993) 1–7.
[5] A. Borodzinski, Catal. Lett. 63 (1999) 35–42.
[6] A. Borodzinski, A. Golebiowski, Langmuir 13 (1997) 883–887.
[7] D. Duca, F. Arena, A. Parmaliana, G. Deganello, Appl. Catal. A – Gen. 172 (1998) 207–216.
[8] D. Duca, F. Frusteri, A. Parmaliana, G. Deganello, Appl. Catal. A – Gen. 146 (1996) 269–284.
[9] W.T. McGown, C. Kemball, D.A. Whan, J. Catal. 51 (1978) 173–184.
[10] W.T. McGown, C. Kemball, D.A. Whan, M.S. Scurrell, J. Chem. Soc. Faraday Trans. I 73 (1977) 632–647.
[11] H.R. Aduriz, P. Bodnariuk, M. Dennehy, C.E. Gigola, Appl. Catal. 58 (1990) 227–239.
[12] A. Borodzinski, Catal. Lett. 71 (2001) 169–175.
[13] C.E. Gigola, H.R. Aduriz, P. Bodnariuk, Appl. Catal. 27 (1986) 133–144.
[14] A. Sarkany, A. Horvath, A. Beck, Appl. Catal. A – Gen. 229 (2002) 117–125.
[15] A. Borodzinski, Pol. J. Chem. 69 (1995) 111–117.
[16] A. Borodzinski, Pol. J. Chem. 72 (1998) 2455–2462.
[17] M. Larsson, J. Jansson, S. Asplund, J. Catal. 162 (1996) 365–367.
[18] M. Larsson, J. Jansson, S. Asplund, J. Catal. 178 (1998) 49–57.
[19] A. Sarkany, J. Catal. 180 (1998) 149–152.
[20] A. Sarkany, React. Kinet. Catal. Lett. 74 (2001) 299–307.
[21] D. Teschner, J. Borsodi, A. Wootsch, Z. Revay, M. Havecker, A. Knop-Gericke, S.D. Jackson, R. Schlogl, Science 320 (2008) 86–89.
[22] D. Teschner et al., J. Catal. 242 (2006) 16.
[23] D. Teschner, Z. Revay, J. Borsodi, M. Havecker, A. Knop-Gericke, R. Schlogl, D. Milroy, S.D. Jackson, D. Torres, P. Sautet, Angew. Chem., Int. Ed. 47 (2008) 9274–9278.
[24] R.M. Lambert, R.M. Ormerod, Mater. Chem. Phys. 29 (1991) 105–115.
[25] A.S. Al-Ammar, G. Webb, J. Chem. Soc. Faraday Trans. I 75 (1979) 1900–1911.
[26] N. Lopez, B. Bridier, J. Perez-Ramirez, J. Phys. Chem. C 112 (2008) 9346–9350.
[27] Y.H. Park, G.L. Price, Ind. Eng. Chem. Res. 30 (1991) 1700–1707.
[28] Y.H. Park, G.L. Price, Ind. Eng. Chem. Res. 30 (1991) 1693–1699.
[29] T.T.P. Cheung, M.M. Johnson, US Patent 5583274, 1996.
[30] T.T.P. Cheung, M.M. Johnson, S.H. Brown, S.A. Zisman, J.B. Kimble, US Patent 5488024, 1996.
[31] S. Gonzalez, K.M. Neyman, S. Shaikhutdinov, H.J. Freund, F. Illas, J. Phys. Chem. C 111 (2007) 6852–6856.
[32] Y. Jin, A.K. Datye, E. Rightor, R. Gulotty, W. Waterman, M. Smith, M. Holbrook, J. Maj, J. Blackson, J. Catal. 203 (2001) 292–306.
[33] N.A. Khan, S. Shaikhutdinov, H.J. Freund, Catal. Lett. 108 (2006) 159–164.
[34] F. Studt, F. Abild-Pedersen, T. Bligaard, R.Z. Sorensen, C.H. Christensen, J.K. Norskov, Angew. Chem., Int. Ed. 47 (2008) 9299–9302.
[35] F. Studt, F. Abild-Pedersen, T. Bligaard, R.Z. Sorensen, C.H. Christensen, J.K. Norskov, Science 320 (2008) 1320–1322.
[36] Q.W. Zhang, J. Li, X.X. Liu, Q.M. Zhu, Appl. Catal. A – Gen. 197 (2000) 221–228.
[37] N.A. Khan, A. Uhl, S. Shaikhutdinov, H.J. Freund, Surf. Sci. 600 (2006) 1849–1853.
[38] D.C. Huang, K.H. Chang, W.F. Pong, P.K. Tseng, K.J. Hung, W.F. Huang, Catal. Lett. 53 (1998) 155–159.
[39] P.A. Sheth, M. Neurock, C.M. Smith, J. Phys. Chem. B 109 (2005) 12449–12466.
[40] G.C. Bond, D.A. Dowden, N. MacKenzie, Trans. Faraday Soc. 54 (1958) 1537–1546.
[41] S. Azad, M. Kaltchev, D. Stacchiola, G. Wu, W.T. Tysoe, J. Phys. Chem. B 104 (2000) 3107–3115.
[42] H. Molero, B.F. Bartlett, W.T. Tysoe, J. Catal. 181 (1999) 49–56.
[43] D. Stacchiola, S. Azad, L. Burkholder, W.T. Tysoe, J. Phys. Chem. B 105 (2001) 11233–11239.
[44] D. Stacchiola, M. Kaltchev, G. Wu, W.T. Tysoe, Surf. Sci. 470 (2000) L32–L38.
[45] E.W. Hansen, M. Neurock, J. Catal. 196 (2000) 241–252.
[46] D.H. Mei, E.W. Hansen, M. Neurock, J. Phys. Chem. B 107 (2003) 798–810.
[47] M. Neurock, D.H. Mei, Top. Catal. 20 (2002) 5–23.
[48] D. Mei, P.A. Sheth, M. Neurock, C.M. Smith, J. Catal. 242 (2006) 1–15.
[49] J. Horiuti, M. Polanyi, Trans. Faraday Soc. 30 (1934) 1164.
[50] J. Gates, L. Kesmodel, Surf. Sci. 120 (1982) L461–L467.
[51] J. Gates, L. Kesmodel, Surf. Sci. 124 (1983) 68–86.
[52] W. Tysoe, G. Nyberg, R. Lambert, Surf. Sci. 135 (1983) 128–146.
[53] I. Jungwirthova, L.L. Kesmodel, Surf. Sci. 470 (2000) L39–L44.
[54] I. Jungwirthova, L.L. Kesmodel, J. Phys. Chem. B 105 (2001) 674–680.
[55] T.V.W. Janssens, S. Volkening, T. Zambelli, J. Wintterlin, J. Phys. Chem. B 102 (1998) 6521–6528.
[56] V. Pallassana, M. Neurock, V.S. Lusvardi, J.J. Lerou, D.D. Kragten, R.A. van Santen, J. Phys. Chem. B 106 (2002) 1656–1669.
[57] P.A. Sheth, M. Neurock, C.M. Smith, J. Phys. Chem. B 107 (2003) 2009–2017.
[58] A. Borodzinski, A. Cybulski, Appl. Catal. A 198 (2000) 51–66.
[59] G. Kresse, J. Hafner, J. Phys. – Condes. Matter 6 (1994) 8245–8257.
[60] G. Kresse, J. Furthmuller, Phys. Rev. B 54 (1996) 11169–11186.
[61] M. Neurock, J. Catal. (2003) 73–88.
[62] M. Neurock, D.H. Mei, Top. Catal. 20 (2002) 5–23.
[63] M. Neurock, V. Pallassana, R.A. van Santen, J. Am. Chem. Soc. 122 (2000) 1150–1153.
[64] E. Hansen, M. Neurock, J. Phys. Chem. B 105 (2001) 9218–9229.
[65] E.W. Hansen, M. Neurock, Surf. Sci. 464 (2000) 91–107.
[66] L.D. Kieken, M. Neurock, D.H. Mei, J. Phys. Chem. B 109 (2005) 2234–2244.
[67] D.H. Mei, Q.F. Ge, M. Neurock, L. Kieken, J. Lerou, Mol. Phys. 102 (2004) 361–369.
[68] G. Henkelman, B.P. Uberuaga, H. Jonsson, J. Chem. Phys. 113 (2000) 9901–9904.
[69] T.A. Halgren, J. Comput. Chem. 17 (1996) 520–552.
[70] R.I. Masel, Principles of Adsorption and Reaction on Solid Surfaces, John Wiley & Sons Inc., New York, 1996.
[71] J.A. Dumesic, D.F. Rudd, L.M. Aparicio, J.E. Rekoske, A.A. Trevino, The Microkinetics of Hydrogeneous Catalysis, Washington, 1993, pp. 39–42.
[72] J. Rekoske, R. Cortright, S. Goddard, S. Sharma, J. Dumesic, J. Phys. Chem. 96 (1992) 1880–1888.
[73] R. Cortright, S. Goddard, J. Reskoske, J. Dumesic, J. Catal. 127 (1991) 342–353.
[74] L.Z. Gva, K.E. Kho, Kinet. Catal. 29 (1988) 331–335.
[75] A. Molnar, A. Sarkany, M. Varga, J. Mol. Catal. A 173 (2001) 185–221.
[76] T.P. Beebe, J.T. Yates, J. Am. Chem. Soc. 108 (1986) 663–671.
[77] T.P. Beebe, M.R. Albert, J.T. Yates, J. Catal. 96 (1985) 1–11.
[78] H. Zea, K. Lester, A.K. Datye, E. Rightor, R. Gulotty, W. Waterman, M. Smith, Appl. Catal. A – Gen. 282 (2005) 237–245.
[79] Y. Inoue, I. Yasumori, J. Phys. Chem. 75 (1971) 880–887.